

Room temperature quantum memory and scalable single photon source based on motional averaging

J. Borregaard,¹ M. Zugenmaier,¹ J. M. Petersen,¹ H. Shen,¹
G. Vasilakis,¹ K. Jensen,¹ E. S. Polzik,¹ and A. S. Sørensen¹

¹*The Niels Bohr Institute, University of Copenhagen,
Blegdamsvej 17, DK-2100 Copenhagen Ø, Denmark*

(Dated: September 3, 2022)

Quantum interfaces between photons and ensembles of atoms have emerged as powerful tools for quantum technologies. High fidelity storage and retrieval of a photon in a collective quantum state of many atoms requires long-lived collective superposition states typically achieved with immobilized atoms. Thermal atomic vapors, which present a simple and scalable resource, have been so far only used for continuous variable processing or for discrete variable processing on short time scales where atomic motion is negligible. We develop a theory based on the concept of motional averaging to enable room temperature discrete variable quantum memories and coherent single photon sources. We show that by choosing the interaction so that atoms can cross the light beam several times during the interaction and by suitable spectral filtering, we erase the “which atom” information and obtain an efficient and homogenous coupling between all atoms and the light. Heralded single excitations can thus be created and stored as collective spinwaves, which can later be read out to produce coherent single photons in a scalable fashion. We demonstrate the feasibility of this approach to scalable quantum memories with a proof of principle experiment with room temperature atoms contained in microcells with spin protecting coating, placed inside an optical cavity.

PACS numbers: 32.80.Qk, 42.50.Ex, 42.50.Pq, 03.67.Bg, 42.50.Pq, 03.67.Hk

Quantum systems can potentially enable highly secure communication [1–4] and powerful quantum computation [5–7]. A major challenge in the construction of reliable quantum technology is to find suitable quantum systems to encode information in. Single photons are ideal information carriers for quantum communication. Nonetheless, the information needs to be stored in a quantum memory in order for the information to be processed [3, 8]. Ensembles of cold atoms have previously been considered for quantum memories since the large number of atoms enables a strong light-atom interaction [9–12]. Cold atoms, however, require extended cooling apparatus, which makes the scalability of such systems challenging. Room temperature atoms allow for a range of operations with continuous variables [13] but the efficiency of such systems for discrete variables is limited by the incoherent atomic motion. Here, we introduce room temperature microcells as a new system for ensemble-based quantum information processing and show theoretically how they may be employed to realize long distance quantum communication in DLCZ-like repeater protocols [3, 4, 14]. The scalability of the system compared to cryogenic systems opens up the possibility of employing spatial multiplexing [15] to greatly enhance the communication rate and reduce the required memory time. As opposed to previous ensemble-based experiments with discrete variables encoded in moving atoms [16], which typically rely on performing operations sufficiently fast that the atoms remain inside the laser beams, we introduce motional averaging, where atoms move in and out of the beam many times during the interaction. Atoms return

back into the beam after colliding with a cell wall without losing the phase information, due to the spin-preserving coating of the walls [17]. This novel approach to photon counting experiments alleviates the effect of atomic motion and can be seen as “trapping” coherent spins in a box-like potential of coated walls. We present a proof of principle experiment demonstrating the effect. Besides the specific experimental realization described here, the ideas leading to the motional averaging are generally applicable and may be used also in other systems where fluctuations of the coupling strength is an issue, such as ion crystals [18].

We consider a setup where an ensemble of atoms with a Λ -scheme level structure is kept in a small cell, coated with an alkene coating [17] (see Fig. S9). In proof-of-principle experiments with an average time between collisions with walls of $\sim 1.4 \mu\text{sec}$ (see below), an atomic coherence time of 10 ms was measured, making the cells suitable as quantum memories [19]. The ensemble is kept at room temperature and, to enhance the interaction with the light, the cell is placed inside a single-sided optical cavity (*cell-cavity*) [20]. In the proof-of-principle experiment a finesse of 17 has been set by the output mirror transmission of 20% and the reflection losses on the cell windows. The light leaving the cell-cavity is coupled into another high finesse cavity, which we shall refer to as the *filter-cavity*. The purpose of this cavity is described below.

Initially the atoms are pumped to the state $|0\rangle$ (see Fig. S9). The objective is to create a single, collective excitation in the ensemble, thereby creating the sym-

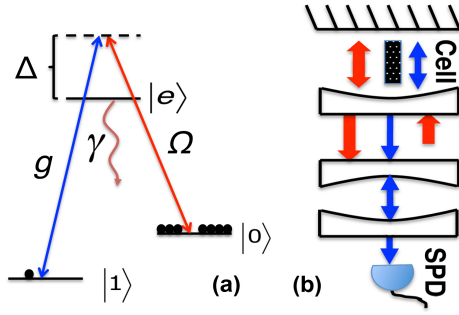


FIG. 1. Sketch of (a) the atomic level structure and (b) the experimental setup for creating a symmetric Dicke state. (a) We assume that all atoms are initially pumped to state $|0\rangle$. The transition $|0\rangle \rightarrow |e\rangle$ is driven by a weak laser field (Rabi frequency Ω) while the cavity mode couples $|e\rangle$ and $|1\rangle$ with a coupling strength g . (b) The atomic ensemble is kept in a small cell inside a single-sided cavity with a low finesse (cell-cavity). The quantum photon (thin arrows) is coupled from the cell-cavity into a high finesse cavity (filter-cavity), which separates it from the classical field (thick arrows) and averages over the atomic motion. The output of the filter-cavity is measured with a single photon detector (SPD) and a single click heralds the creation of an approximate Dicke state in the ensemble.

metric Dicke state $|\psi_D\rangle = \hat{S}_D|00\dots 0\rangle$, where $\hat{S}_D = \frac{1}{\sqrt{N}} \sum_j |1\rangle_j \langle 0|$ and N is the number of atoms in the ensemble. This is called the write process. To obtain the single excitation, the $|0\rangle \rightarrow |e\rangle$ transition is driven with a laser pulse, which is far-detuned from the atomic transition to suppress the Doppler broadening of the atomic levels and absorption (see [19]) and sufficiently weak that multiple excitations in the ensemble can be neglected. The process is conditioned on detecting single photons emitted in a Raman transition from $|0\rangle \rightarrow |1\rangle$, referred to as the quantum photon. Upon detection, the atomic state is projected into the symmetric Dicke state if the light experienced a homogeneous interaction with all atoms, i.e. if the probability for different atoms to have emitted the photon is equal. In a realistic setup, the laser beam does not fill the entire cell and only atoms that are in the beam contribute to the cavity field. Atoms leaving the beam will return to the beam due to the frequent collisions with the cell walls and we exploit this to make a motional averaging of the light-atom interaction. During the collisions, the atomic state is preserved due to the alkene coating of the cells. If the interaction time is long enough to allow the atoms to move in and out of the beam several times, they will on average have experienced the same interaction with the light. Consequently, the detection of a cavity photon will, to a good approximation, project the atomic state to a Dicke state. Since the cell-cavity has a limited finesse, it may, in practice, not have a sufficiently narrow linewidth to allow this averaging. We therefore introduce the filter-cavity. As we show be-

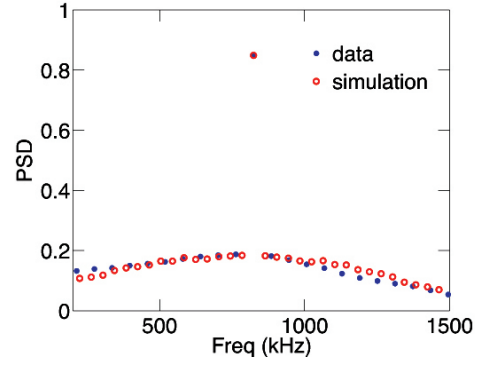


FIG. 2. Experimental data and simulation of the power spectral density (PSD) of the atomic spin noise. The details of the simulation are described in the supplemental material [19]. The broad feature originates from short-time, incoherent light-atom interaction while the sharp peak is the long-time, coherent light-atom interaction. The data is centered around the Larmor frequency, which was 823.8 kHz. The optical readout was obtained through the Faraday effect (see [19] for details). The cell used in the experiment had dimensions $2L \times 2L \times 2L_z$ with $L = 150 \mu\text{m}$ and $L_z = 0.5 \text{ cm}$. The light beam had a Gaussian profile with a waist of $55 \mu\text{m}$.

low the output from the cell-cavity consists of a spectrally narrow coherent component and a broad incoherent component (see Fig. 2 and Ref. [19]). By selecting out the coherent part, the filter-cavity effectively increases the interaction time and allows for motional averaging. The filter-cavity can also separate the quantum photon from the classical drive if there is a small frequency difference between the two such that only one frequency is resonant in the filter-cavity while both are sustained in the cell-cavity. After a successful creation of an excitation in the ensemble, the state can be kept until read out. In the readout process a long classical pulse addresses the $|1\rangle \rightarrow |e\rangle$ transition such that the single excitation is converted into a photon on the $|e\rangle \rightarrow |0\rangle$ transition (with g and Ω interchanged in Fig. 1a). This pulse should be long enough to allow for motional averaging as in the write process.

The quality of our system, when considered as a part of a quantum repeater, is characterized by both the efficiency of the write and readout processes and the quality of the single photons being retrieved. We first go through the details of the setup shown in Fig. 1b to derive the efficiency of the write and readout processes and later discuss the quality of the photons. The Hamiltonian, describing the write process, is ($\hbar = 1$)

$$\hat{H} = \sum_{j=1}^N -\Delta \hat{\sigma}_{ee}^{(j)} - \left(\frac{\Omega_j(t)}{2} \hat{\sigma}_{e0}^{(j)} + g_j(t) \hat{a}_{\text{cell}} \hat{\sigma}_{e1}^{(j)} + \text{H.c.} \right), \quad (1)$$

where $\Delta = \omega_{\text{laser}} - \omega_{e0}$ with ω_{laser} being the frequency of the driving laser and ω_{e0} being the transition frequency between the levels $|e\rangle$ and $|0\rangle$. Ω_j (g_j) charac-

terizes the coupling between the laser (cavity) field and the j 'th atom. The field in the cell-cavity is described by the annihilation operator \hat{a}_{cell} and we have defined the atomic operators $\sigma_{mn}^{(j)} = |m\rangle_j \langle n|$ for the j 'th atom, where $\{m, n\} \in \{0, 1, e\}$. To obtain an expression for the cavity field, we formally integrate Heisenberg's equations of motion including the cavity (κ_1) and atomic (γ) decays [21]. The field at the detector (see Fig. 1b), described by \hat{a} , is found by propagating \hat{a}_{cell} through the filter-cavity. Treating the interaction as a perturbation to the atomic system, we find (see Ref. [19])

$$\hat{a} = i \frac{\kappa_2 \sqrt{\kappa_1}}{2} \sum_{j=1}^N \theta_j(t) \hat{\sigma}_{10}^{(j)}, \quad (2)$$

where

$$\theta_j(t) = \frac{1}{2} \int_0^t dt' \int_0^{t'} dt'' \int_0^{t''} dt''' e^{-\kappa_2(t-t')/2} e^{-\kappa_1(t'-t'')/2} \times e^{-(\gamma/2 - i\Delta)(t''-t''')} g_j^*(t'') \Omega_j(t'''), \quad (3)$$

with κ_2 being the decay rate of the filter-cavity. In deriving the above equations, we have neglected the intracavity losses. The efficiency is defined as the probability of having stored a single excitation in the symmetric Dicke state upon detection of a quantum photon. Neglecting higher order excitations, the atomic state is projected to $\sqrt{p(t)}|\psi_a(t)\rangle = \sqrt{\eta} {}_I\langle 0|\hat{a}(t)|00\dots 0\rangle|0\rangle_I$ when the quantum photon is detected at time t . Here, $|0\rangle_I$ is the vacuum of the light in the cavity mode and $p(t)$ is the probability density of detecting the photon at time t with η being the single photon detection efficiency. Assuming that the driving pulse has a length of t_{int} , we can calculate the efficiency of the write process as

$$\eta_{\text{write}} = \frac{\int_0^{t_{\text{int}}} p(t) |\langle \psi_D | \psi_a(t) \rangle|^2 dt}{\int_0^{t_{\text{int}}} p(t) dt} \approx \frac{\int_0^{t_{\text{int}}} |\langle \theta_j(t) \rangle_e|^2 dt}{\int_0^{t_{\text{int}}} \langle |\theta_j(t)|^2 \rangle_e dt}, \quad (4)$$

where we have used Eq. (2) assuming $N \gg 1$ and have defined the ensemble average $\langle \dots \rangle_e = \frac{1}{N} \sum_{j=1}^N \langle \dots \rangle$ [19]. In order to evaluate the efficiency, we write the time dependent couplings as $g_j(t) = g_{xy}^{(j)}(t) \sin(k_q z_j(t))$ and $\Omega_j(t) = \Omega_{xy}^{(j)}(t) \sin(k_c z_j(t))$, where we now explicitly include the spatial dependence of the couplings. The xy -dependence is assumed to be Gaussian. The z dependence is sinusoidal due to the standing wave in the cavity. k_q (k_c) is the wave vector associated with the quantum photon (classical field). Furthermore, we adiabatically eliminate the integral over t''' appearing in Eq. (3), assuming the xy -couplings to be constant on a timescale of $1/\Delta$ and that $z_j(t''') = z_j(0) + v_z^{(j)} t'''$, where $v_z^{(j)}$ is the z -component of the velocity of the j 'th atom. $v_z^{(j)}$ is also assumed to be constant on this timescale since a

change in $v_z^{(j)}$ requires a collision with a cell wall. Note that $|\langle \theta_j(t) \rangle|^2$ does not contain any correlations between an atom's position at different times, whereas $\langle |\theta_j(t)|^2 \rangle$ does. Eq. (S17) thus characterizes the effect of the random atomic motion and the motional averaging associated with it. We evaluate $|\langle \theta_j(t) \rangle|^2$ assuming that the atoms are evenly distributed in a cell with dimensions $2L \times 2L \times 2L_z$ with $L_z \gg L$ and that they are in thermal equilibrium with the walls at room temperature [19]. The correlations decay in time such that after many collisions with the walls, an atom's position is completely uncorrelated from its initial position. We assume that the decay of the correlations is exponential such that, e.g., $\langle g_{xy}^{(j)}(0) g_{xy}^{(j)}(t) \rangle = \langle (g_{xy}^{(j)}(0))^2 \rangle e^{-\Gamma t} + \langle g_{xy}^{(j)}(0) \rangle^2 (1 - e^{-\Gamma t})$, where the first term contains the short time correlations while the second term characterizes the long time limit where the correlations are only through the average values. We substantiate this assumption by simulating a box of randomly moving, non-interacting atoms and find good agreement with a decay rate $\Gamma = \alpha v_{\text{thermal}}/w$ where v_{thermal} is the average thermal velocity of the atoms, w is the waist of the Gaussian cavity mode and α is a numerical constant on the order of unity [19]. Employing this model for the atomic correlations and assuming $\kappa_2 t_{\text{int}} \gg 1$ such that the effective interaction time ($1/\kappa_2$) is set by the linewidth of the filter-cavity, we find that

$$\eta_{\text{write}} \approx \frac{1}{1 + \frac{\kappa_2}{2\Gamma + \kappa_2} \left(\frac{4L^2}{\pi w^2} - 1 \right)} \approx 1 - \frac{1}{N_{\text{pass}}}, \quad (5)$$

where we have assumed that $\kappa_1 \gg (\Gamma, \kappa_2)$ and that we are detuned beyond the Doppler width of the atomic levels. Furthermore, we have assumed that $w < L$. Eq. (5) shows that $\eta_{\text{write}} \rightarrow 1$ as $\kappa_2/\Gamma \rightarrow 0$, i.e., the write efficiency improves with the length of the effective interaction time. This is the motional averaging of the atomic interaction with the light. Eq. (5) also shows how the efficiency improves as the ratio between the beam area and the cell area ($\pi w^2/L^2$) increases. The last equality in Eq. (5) is obtained assuming that $\Gamma \gg \kappa_2$. Here $N_{\text{pass}} \approx \frac{\Gamma w^2}{\kappa_2 L^2}$ is the number of passes of an atom through the beam during the interaction.

The validity of the model has been tested by comparison to the experimental observation of the spectral density of the atomic spin noise (see [19] for details). For this experiment, atoms have been prepared in a coherent spin state and spin noise is measured by Faraday rotation [13]. In the weak probing limit this is equivalent to probing the emitted light. Fig. 2 shows an excellent agreement between the experiment and the model. The narrow peak is due to the atoms, which repeatedly come back into the beam with the same spin phase, whereas the broad background is due to the single transient through the beam. With a filter cavity we would select only the narrow peak resulting in a highly coherent atomic state. To qualitatively describe the write efficiency, we have simulated the

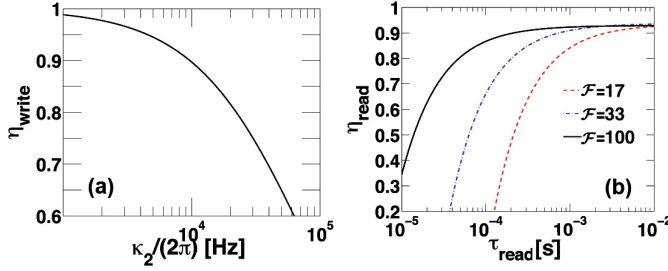


FIG. 3. (a) Write efficiency as a function of the linewidth of the filter-cavity. We have simulated a Cs-cell with $L = 150 \mu\text{m}$ and $w = 55 \mu\text{m}$ corresponding to the cells being used in the experiment. We have assumed a detuning of $\Delta \sim 2\pi \cdot 900$ MHz, a pulse length of $t_{\text{int}} = 10/\kappa_2$ and $\kappa_1 = 2\pi \cdot 46$ MHz. (b) Readout efficiency plotted against the readout time τ_{read} for different values of the finesse (\mathcal{F}) of the cell-cavity. The efficiency was simulated for the same Cs-cells as the write efficiency and we have assumed that $\tau_{\text{read}} = 3/\Gamma_{\text{read}}$ where Γ_{read} is the readout rate, which is proportional to the classical drive. The optical depth was assumed to be 84, which was measured in the experiment [19]. In the simulations we have included the full level structure of ^{133}Cs .

experiment with the Cs-cells [19]. Fig. 3a shows the write efficiency plotted against the linewidth of the filter-cavity. It is seen that $\eta_{\text{write}} \approx 90\%$ for $\kappa_2 \approx 2\pi \cdot 10$ kHz, which translates into a write time of $\sim 150 \mu\text{s}$.

We will now consider the readout process. We assume that a single excitation has been stored in the ensemble and a classical drive (Ω) is then applied in order to read out the excitation as a cavity photon. The Hamiltonian is obtained by interchanging $\hat{\sigma}_{e0}^{(j)}$ and $\hat{\sigma}_{e1}^{(j)}$ in Eq. (1). From Heisenberg's equations of motion, we obtain a set of $N + 1$ coupled differential equations of the cavity field \hat{a}_{cell} and the atomic operators $\hat{\sigma}_{01}^{(j)}$. The equations can be expressed as a matrix system of the form

$$\frac{d\mathbf{x}(t)}{dt} = \mathbf{M}(t)\mathbf{x}(t), \quad (6)$$

where $\mathbf{x}(t) = (\hat{a}_{\text{cell}}, \hat{\sigma}_{01}^{(1)}, \hat{\sigma}_{01}^{(2)}, \dots, \hat{\sigma}_{01}^{(N)})$ and $\mathbf{M}(t)$ is the coupling matrix between the atoms and the cavity field. Assuming a weak laser pulse, we write the couplings as $\Omega_j(t) = \langle \Omega \rangle + \delta\Omega_j(t)$ where $\langle \Omega \rangle$ is the average, time-independent coupling of the atoms. The coupling of an atom is thus viewed as consisting of a (large) homogeneous part and a (small) inhomogeneous perturbation. The coupling matrix is then expressed as $\mathbf{M}(t) = \mathbf{M}_0 + \delta\mathbf{M}(t)$ where \mathbf{M}_0 contains the average and time-independent couplings while $\delta\mathbf{M}(t)$ contains the time dependent perturbations. Assuming that the readout pulse is long, the atoms will have had the same average interaction with the light meaning that $\mathbf{M}(t) \approx \mathbf{M}_0$. Treating $\delta\mathbf{M}(t)$ as a perturbation, we obtain a perturbative expansion of \hat{a}_{cell} . The readout efficiency is $\eta_{\text{read}} = \int_0^{\tau_{\text{read}}} dt \kappa_1 \langle \hat{a}_{\text{cell}}^\dagger(t) \hat{a}_{\text{cell}}(t) \rangle$, where the

factor of κ_1 ensures the right normalization. To lowest order, we find that

$$\eta_{\text{read},0} \approx \frac{1}{\frac{\pi}{d\mathcal{F}} + 1} \quad (7)$$

where d is the optical depth on the $|0\rangle \leftrightarrow |e\rangle$ transition and \mathcal{F} is the finesse of the cell-cavity. Eq. (7) is equivalent to the result for cold atomic ensembles [21] and represents the long time limit of perfect motional averaging where the efficiency improves with optical depth and finesse of the system.

Nonetheless, the coherence time of real atoms is limited and a fast readout is therefore desirable. When increasing the strength of the readout pulse, we need to consider higher order terms in the perturbative expansion of $\hat{a}_{\text{cell}}(t)$. To second order, we find that $\eta_{\text{read}} \sim \eta_{\text{read},0} + \eta_{\text{read},2}$ where the second order term ($\eta_{\text{read},2}$) mainly describes the loss of the excitation due to spontaneous emission. Consequently, the magnitude of $\eta_{\text{read},2}$ increases with the driving strength. As for the write efficiency, we have simulated the readout process based on the Cs-cells [19]. Fig. 3b shows the readout efficiency for different values of the finesse as a function of the readout time. The Cs-cells have a measured optical depth around 84, which means that for a finesse of 100, a readout efficiency of $\eta_{\text{read}} \approx 90\%$ can be obtained for a readout time of $t \approx 183 \mu\text{s}$. In the simulations, we have included the full level structure of ^{133}Cs .

We will now consider, which errors limit the performance of the system when being a part of a DLCZ repeater protocol [3]. The dominant errors in our setup are multiple excitations during the write process, dark counts and inefficient optical pumping in the preparation of the initial state [19]. For a dark count rate of 1 Hz and SPD detection efficiency of 95% [22, 23], we consider a basic DLCZ repeater with a single entanglement swap and a distance of 80 km. Including various experimental imperfections, we estimate that a pair with fidelity $\sim 80\%$ can be distributed with a rate of ~ 0.2 Hz [19]. Note that we have neglected effects from limited memory time and have assumed an optical pumping inefficiency of 0.08%. The rate of entanglement distribution can, however, be greatly enhanced using spatially multiplexing schemes, which are possible due to the scalable nature of the room temperature cells. Multiplexing will also decrease the necessary memory time [15].

In conclusion, we have introduced the concept of motional averaging, which can be used to make efficient and scalable single photon sources based on atomic ensembles at room temperature. We have demonstrated the concept in a specific setup where the atomic ensemble is kept in a small cell inside a cavity and shown how both read and write efficiencies above 90% can be achieved for a real experimental system based on Cs-atoms. To verify this effect we have performed a proof-of-principle experiment

with room temperature Cs atoms contained in a micro-cell with spin preserving coating deposited on the walls. The measurement of the atomic ensemble spin noise reveals the coherent nature of the spin dynamics, resulting in a narrow peak which is in excellent agreement with the theoretical model being used. As a consequence the room temperature cells emerge as a promising building block for future quantum networks. The scalable nature of room-temperature systems based on motional averaging may also be used for scalable photonic quantum simulators [24–26].

The research leading to these results has received funding from the Lundbeck Foundation, the European Research Council under the European Union’s Seventh Framework Programme (FP/2007-2013) / ERC Grant Agreement n. 306576, the ERC grant INTERFACE, the U. S. ARO under the grant W911NF-11-0235 and the EU project MALICIA. K. Jensen acknowledges support from the Carlsberg Foundation.

-
- [1] J. I. Cirac, P. Zoller, H. J. Kimble, and H. Mabuchi, *Phys. Rev. Lett.* **78**, 3221 (1997).
 - [2] H. J. Kimble, *Nature* **453**, 1023 (2008).
 - [3] L.-M. Duan, M. D. Lukin, J. I. Cirac, and P. Zoller, *Nature* **414**, 413 (2001).
 - [4] N. Sangouard, C. Simon, B. Zhao, Y.-A. Chen, H. de Riedmatten, J.-W. Pan, and N. Gisin, *Phys. Rev. A* **77**, 062301 (2008).
 - [5] T. D. Ladd, F. Jelezko, R. Laflamme, Y. Nakamura, C. Monroe, and J. L. O’Brien, *Nature* **464**, 45 (2010).
 - [6] R. P. Feynman, *Int. J. Theor. Phys.* **21**, 467 (1982).
 - [7] P. W. Shor, *SIAM J. Comput.* **26**, 1484 (1997).
 - [8] H.-J. Briegel, W. Dür, J. I. Cirac, and P. Zoller, *Phys. Rev. Lett.* **81**, 5932 (1998).
 - [9] J. Simon, H. Tanji, J. K. Thompson, and V. Vuletić, *Phys. Rev. Lett.* **98**, 183601 (2007).
 - [10] C.-W. Chou, L. Laurat, H. Deng, K. S. Choi, H. de Riedmatten, D. Felinto, and H. J. Kimble, *Science* **316**, 1316 (2007).
 - [11] Y.-A. Chen, S. Chen, Z. S. Yuan, B. Zhao, C. S. Chu, J. Schmiedmayer, and J.-W. Pan, *Nature Physics* **4**, 103 (2008).
 - [12] A. V. Gorshkov, A. André, M. Fleischhauer, A. S. Sørensen, and M. D. Lukin, *Phys. Rev. Lett.* **98**, 123601 (2007).
 - [13] K. Hammerer, A. S. Sørensen, and E. S. Polzik, *Rev. Mod. Phys.* **82**, 1041 (2010).
 - [14] L. Jiang, J. M. Taylor, and M. D. Lukin, *Phys. Rev. A* **76**, 012301 (2007).
 - [15] O. A. Collins, S. D. Jenkins, A. Kuzmich, and T. A. B. Kennedy, *Phys. Rev. Lett.* **98**, 060502 (2007).
 - [16] M. Hosseini, G. Campbell, B. M. Sparkes, P. K. Lam, and B. C. Buchler, *Nature Physics* **7**, 794 (2011).
 - [17] M. V. Balabas, T. Karaulanov, M. P. Ledbetter, and D. Budker, *Phys. Rev. Lett.* **105**, 070801 (2010).
 - [18] P. Herskind, A. Dantan, M. B. Langkilde-Lauesen, A. Mortensen, J. L. Sørensen, and M. Drewsen, *App. Phys. B* **93**, 373 (2008).
 - [19] See Supplemental Material starting at page 6
 - [20] G. Vasilakis, H. Shen, K. Jensen, M. Balabas, D. Salart, B. Chen, and E. S. Polzik, arXiv:1411.6289 (2014).
 - [21] A. V. Gorshkov, A. André, M. D. Lukin, and A. S. Sørensen, *Phys. Rev. A* **76**, 033804 (2007).
 - [22] A. E. Lita, A. J. Miller, and S. W. Nam, *Optics Express* **16**, 3032 (2008).
 - [23] D. H. Smith, G. Gillett, M. P. de Almeida, C. Branciard, A. Fedrizzi, T. J. Weinhold, A. Lita, B. Calkins, T. Gerrits, H. M. Wiseman, S. W. Nam, and A. G. White, *Nature Communications* **3**, 625 (2012).
 - [24] A. Aspuru-Guzik and P. Walther, *Nature Physics* **8**, 285 (2011).
 - [25] S. Aaronson and A. Arkhipov, *Proceedings of the 43rd Annual ACM Symposium on Theory of Computing*, 333 (2011).
 - [26] M. Tillmann, B. Dakić, R. Heilmann, S. Nolte, A. Szameit, and P. Walther, *Nature photonics* **7**, 540 (2011).
 - [27] J. M. Petersen, *An Ion Crystal Quantum Repeater*, Master’s thesis, The Niels Bohr Institute, University of Copenhagen (2010).
 - [28] A. V. Gorshkov, A. André, M. D. Lukin, and A. S. Sørensen, *Phys. Rev. A* **76**, 033804 (2007).
 - [29] A. V. Gorshkov, A. André, M. Lukin, and A. Sørensen, *Phys. Rev. A* **76**, 033806 (2007).
 - [30] J. D. Jackson, *Classical Electrodynamics* (John Wiley and Sons, Inc., 1975).
 - [31] K. Jensen, *Quantum Information, Entanglement and Magnetometry with macroscopic Gas Samples and Non-Classical Light*, Ph.D. thesis, The Niels Bohr Institute, University of Copenhagen (2011).
 - [32] C. K. Hong, Z. Y. Ou, and L. Mandel, *Phys. Rev. Lett.* **59**, 2044 (1987).
 - [33] N. Sangouard, C. Simon, H. de Riedmatten, and N. Gisin, *Rev. Mod. Phys.* **83**, 33 (2011).

SUPPLEMENTAL MATERIAL

In this supplemental material to the article “Room temperature quantum memory and scalable single photon source based on motional averaging”, we describe the details of the write and read processes discussed in the article. We estimate the number of classical photons required to implement the procedure and present the exact definition of the optical depth referred to in the article. Furthermore, we present the details of our numerical simulations and discuss the details of the proof-of-principle experiment described in the article. Finally, we estimate the errors limiting the performance of the proposed setup in a DLCZ-like quantum repeater. We emphasize that many of the calculations are based on similar calculations presented in Ref. [27].

WRITE IN

In this section, we describe the details of the write process. Our starting point is the interaction Hamiltonian in Eq. (1) in the article, which is reproduced below

$$\hat{H}_{\text{write}} = \sum_{j=1}^N -\Delta \hat{\sigma}_{ee}^{(j)} - \left(\frac{\Omega_j(t)}{2} \hat{\sigma}_{e0}^{(j)} + g_j(t) \hat{a}_{\text{cell}} \hat{\sigma}_{e1}^{(j)} + H.c. \right). \quad (\text{S8})$$

From this Hamiltonian, we obtain the equations of motion

$$\frac{d\hat{a}_{\text{cell}}}{dt} = -\frac{\kappa_1}{2} \hat{a}_{\text{cell}} + i \sum_{j=1}^N g_j^*(t) \hat{\sigma}_{1e}^{(j)} + \hat{F}_{\kappa_1} \quad (\text{S9})$$

$$\frac{d\hat{\sigma}_{1e}^{(j)}}{dt} = -\left(\frac{\gamma}{2} - i\Delta\right) \hat{\sigma}_{1e}^{(j)} - ig_j(t) \hat{a}_{\text{cell}} (\hat{\sigma}_{ee}^{(j)} - \hat{\sigma}_{11}^{(j)}) + i \frac{\Omega_j(t)}{2} \hat{\sigma}_{10}^{(j)} + \hat{F}_{1e}^{(j)} \quad (\text{S10})$$

$$\frac{d\hat{\sigma}_{10}^{(j)}}{dt} = -ig_j(t) \hat{a}_{\text{cell}} \hat{\sigma}_{e0}^{(j)} + i \frac{\Omega_j^*(t)}{2} \hat{\sigma}_{1e}^{(j)}, \quad (\text{S11})$$

where we have included the cavity intensity decay with a rate κ_1 and the spontaneous emission of the atoms with a rate γ . Associated with these decays, are corresponding Langevin noise operators, \hat{F}_{κ_1} , for the cavity decay and $\hat{F}_{1e}^{(j)}$ for the atomic decay [28]. Note, that we have neglected dephasing of the atoms, e.g., due to collisions. We assume that all the atoms are initially in the ground state $|0\rangle$ and that the interaction with the light is a small perturbation to the system. We can therefore assume that $\hat{\sigma}_{ee}^{(j)} \approx \hat{\sigma}_{11}^{(j)} \approx 0$. The noise operators describes vacuum noise and will never result in either an atomic or field excitation. Hence, they will never give rise to clicks in the detector (see Fig. 1b in the article) and we can consequently ignore them as described in Ref. [28]. Furthermore, we treat $\hat{\sigma}_{10}(t)$ as slowly varying in time and formally integrate Eqs. (S9) and (S10) to obtain

$$\hat{a}_{\text{cell}}(t') = -\frac{1}{2} \sum_{j=1}^N \int_0^{t'} dt'' \int_0^{t''} dt''' e^{-\kappa_1/2(t'-t'')} e^{-(\gamma/2-i\Delta)(t''-t''')} g_j^*(t'') \Omega_j(t''') \hat{\sigma}_{10}^{(j)}. \quad (\text{S12})$$

To find the field at the detector, we need to propagate the field through the filter-cavity. The input/output relations for the filter-cavity are

$$\frac{d\hat{a}_{\text{filter}}}{dt} = -\frac{\kappa_2}{2} \hat{a}_{\text{filter}} + \sqrt{\kappa_2 \kappa_1 / 2} \hat{a}_{\text{cell}}, \quad (\text{S13})$$

$$\hat{a} = \sqrt{\kappa_2 / 2} \hat{a}_{\text{filter}}, \quad (\text{S14})$$

where κ_2 is the intensity decay rate of the filter-cavity, \hat{a}_{filter} describes the field inside the filter-cavity and \hat{a} describes the field at the detector. We neglect any input noise from the cavity decay since it never gives a click in our detector and we have also neglected intra-cavity losses. Formally integrating Eq. (S13), and using Eq. (S14), gives the expression for the operator \hat{a} shown in Eq. (2) in the article, which is reproduced below

$$\hat{a} = -\frac{\kappa_2 \sqrt{\kappa_1}}{4} \sum_{j=1}^N \theta_j(t) \hat{\sigma}_{10}^{(j)}, \quad (\text{S15})$$

where

$$\theta_j(t) = \int_0^t dt' \int_0^{t'} dt'' \int_0^{t''} dt''' e^{-\kappa_2(t-t')/2} e^{-\kappa_1(t'-t'')/2} e^{-(\gamma/2 - i\Delta)(t''-t''')} g_j^*(t'') \Omega_j(t'''). \quad (\text{S16})$$

We condition the write process on the measurement of a quantum photon at the detector. Consequently, we define the write efficiency, η_{write} , as the conditional overlap between the actual atomic state, $|\psi_a(t)\rangle$, upon detection of a quantum photon at time t (we assume 100% detection efficiency), and the Dicke state $|\psi_D\rangle$. The write efficiency is thus

$$\eta_{\text{write}} = \frac{\int_0^{t_{\text{int}}} p(t) |\langle \psi_D | \psi_a(t) \rangle|^2 dt}{\int_0^{t_{\text{int}}} p(t) dt}, \quad (\text{S17})$$

where $p(t)$ is the probability density of detecting the photon at time t . Inserting Eq. (S15) into Eq. (S17) and treating the interaction as a perturbation to the atomic state, we obtain [27]

$$\eta_{\text{write}} = \frac{\int_0^{t_{\text{int}}} |\langle \theta_j(t) \rangle_e|^2 dt}{\int_0^{t_{\text{int}}} \langle |\theta_j(t)|^2 \rangle_e dt} \frac{N-1}{N} + \frac{1}{N} \approx \frac{\int_0^{t_{\text{int}}} |\langle \theta_j(t) \rangle_e|^2 dt}{\int_0^{t_{\text{int}}} \langle |\theta_j(t)|^2 \rangle_e dt}. \quad (\text{S18})$$

Here we have defined the ensemble average $\langle \dots \rangle_e = \frac{1}{N} \sum_j^N \langle \dots \rangle$ and assumed $N \gg 1$ in the last step. First, we focus on the expression for $\theta_j(t)$ in Eq. (S16) in order to derive a simple expression for η_{write} . To perform the integration over t''' , we assume that the couplings can be expressed as

$$\Omega_j(t''') = \Omega_{xy}^{(j)}(t''') \sin(k_c(z_j(0) + v_z^{(j)}(t'''))) \quad (\text{S19})$$

$$g_j(t'') = g_{xy}(t'') \sin(k_q(z_j(t''))), \quad (\text{S20})$$

where k_c (k_q) is the wavenumber of the classical (quantum) field and $z_j(t)$ ($v_z^{(j)}(t)$) is the z components of the position (velocity) of the j 'th atom at time t . The cavity field is a standing wave along the z -direction and both modes are assumed to have a node at the center of the cell at $z = 0$. This geometry ensures an ideal overlap between the two modes. Note that an ideal overlap could also be obtained with antinodes at $z = 0$ achieved if the two modes differ by an even number of FSR (Free spectral range). The xy -dependence of $\Omega_j(t''')$ ($\Omega_{xy}^{(j)}(t''')$) and the velocity is assumed to be constant for the integration over t''' , i.e., on a time scale of $1/\Delta$ (we assume that $\Delta \gg \gamma$). For atoms at room temperature, we need $\Delta \sim 1$ GHz in order to suppress the effect of the Doppler broadening of the atomic levels. This translates into a time scale of ~ 1 ns. The average velocity of room temperature atoms is ~ 200 m/s and the atoms will thus only move $\sim 0.1 \mu\text{m}$ on this timescale. This is a small distance compared to the transverse size of the beam, which is several μm . It is thus justified to assume that $\Omega_{xy}^{(j)}(t''')$ is constant for the integration over t''' . The z -dependence of the coupling, however, varies rapidly due to the standing wave in the cavity and cannot be assumed to be constant. Nonetheless, the velocity of an atom can be assumed to be constant since a change in the velocity requires a collision with the cell walls. We perform the integration over t''' by adiabatically eliminating the decay of the atoms since we are far detuned. As a result, we find that

$$\begin{aligned} \theta_j(t) = & \frac{-1}{4} \int_0^t dt' \int_0^{t'} dt'' e^{-\kappa_2/2(t-t')} e^{-\kappa_1/2(t'-t'')} (g_{xy}^{(j)}(t''))^* \Omega_{xy}^{(j)}(t'') \\ & \times \left(\frac{e^{-i(k_c - k_q)z_j(t'')} - e^{-i(k_c + k_q)z_j(t'')}}{-\gamma/2 + i(\Delta + k_c v_z^{(j)}(t''))} + \frac{e^{i(k_c - k_q)z_j(t'')} - e^{i(k_c + k_q)z_j(t'')}}{-\gamma/2 + i(\Delta - k_c v_z^{(j)}(t''))} \right). \end{aligned} \quad (\text{S21})$$

To evaluate the write efficiency, we wish to obtain an expression for $\langle \theta_j(t) \rangle$ (see Eq. (S18)). To this end, we assume that the spatial distribution of the atoms is uniform and that the velocity distribution of the atoms follows the Maxwell-Boltzmann distribution with temperature T . Both distributions are assumed to be independent of time. We also assume that $k_c \sim k_q = k$ and that $kL_z \gg 1$ such that $\langle e^{\pm 2ikz} \rangle \approx 0$. Here, $2L_z$ is the length of the cell in the beam direction. The xy -dependence of the couplings are assumed to have the same Gaussian form such that

$$\Omega_{xy}^{(j)}(t) = \Omega e^{-\frac{x_j^2(t) - y_j^2(t)}{w^2}}, \quad (\text{S22})$$

$$g_{xy}^{(j)}(t) = g e^{-\frac{x_j^2(t) - y_j^2(t)}{w^2}}, \quad (\text{S23})$$

where w is the waist of the beams and x_j (y_j) is the x (y) component of the position of the j 'th atom. With these assumptions, we obtain

$$\begin{aligned} \langle \theta_j(t) \rangle_e &= -\frac{1}{4} \int_0^t dt' \int_0^{t'} dt'' e^{-\kappa_2/2(t-t')} e^{-\kappa_1/2(t'-t'')} \langle g_{xy}^*(t'') \Omega_{xy}(t'') \rangle \\ &\quad \times \left\langle \frac{1 - e^{-2ikz_j(t'')}}{-\gamma/2 + i(\Delta + kv_z^{(j)}(t''))} + \frac{1 - e^{2ikz_j(t'')}}{-\gamma/2 + i(\Delta - kv_z^{(j)}(t''))} \right\rangle_e \end{aligned} \quad (\text{S24})$$

$$= \frac{\pi^{3/2} g \Omega}{16 \Gamma_d} \mathbf{w}[(\Delta + i\gamma/2)/\Gamma_d] \frac{w^2}{L^2} \int_0^t dt' \int_0^{t'} dt'' e^{-\kappa_2/2(t-t')} e^{-\kappa_1/2(t'-t'')} \quad (\text{S25})$$

$$= \frac{\pi^{3/2} g \Omega}{4 \Gamma_d} \mathbf{w}[(\Delta + i\gamma/2)/\Gamma_d] \frac{w^2}{L^2} \frac{1}{\kappa_1 \kappa_2}, \quad (\text{S26})$$

where we have assumed that $e^{-(\kappa_1/2)t} \approx e^{-(\kappa_2/2)t} \approx 0$ in going from Eq. (S25) to Eq. (S26). Furthermore, we have assumed that the cell dimensions ($x \times y \times z$) are $2L \times 2L \times 2L_z$ and that $\text{erf}(\sqrt{2}L/w)^2 \approx 1$ meaning that we ignore any small portion of the beam, which is outside the cell. $\mathbf{w}[\dots]$ is the Faddeeva function defined as $\mathbf{w}[z] = e^{-z^2}(1 - \text{erf}(-iz))$ and $\Gamma_d = \sqrt{2k_b T/mk}$ is the Doppler width of the atomic levels at the temperature T where m is the atomic mass and k_b is the Boltzmann constant.

Having obtained an expression for $\langle \theta_j(t) \rangle$, we now focus on $\langle |\theta_j(t)|^2 \rangle$. It follows from Eq. (S21) that

$$\begin{aligned} \langle |\theta_j(t)|^2 \rangle_e &= \frac{1}{16} \int_0^t dt'_1 \int_0^{t'_1} dt''_1 \int_0^{t'_2} dt'_2 \int_0^{t'_2} dt''_2 e^{-\kappa_2/2(t-t'_1)} e^{-\kappa_1/2(t'_1-t''_1)} e^{-\kappa_2/2(t-t'_2)} e^{-\kappa_1/2(t'_2-t''_2)} \\ &\quad \times \langle XY_j^*(t''_1) XY_j(t''_2) Z_j^*(t'_1) Z_j(t'_2) \rangle_e, \end{aligned} \quad (\text{S27})$$

where we have defined

$$XY_j(t) = (g_{xy}^{(j)}(t))^* \Omega_{xy}^{(j)}(t) \quad (\text{S28})$$

$$Z_j(t) = \frac{1 - e^{-2ikz_j(t)}}{-\gamma/2 + i(\Delta + kv_z^{(j)}(t))} + \frac{1 - e^{2ikz_j(t)}}{-\gamma/2 + i(\Delta - kv_z^{(j)}(t))}. \quad (\text{S29})$$

To proceed we write $Z_j(t) = \langle Z \rangle + \delta Z_j(t)$ and $XY_j(t) = \langle XY \rangle + \delta XY_j(t)$, i.e., we assume that the terms consist of large average parts ($\langle Z \rangle, \langle XY \rangle$) and small time-dependent perturbations ($\delta Z_j(t), \delta XY_j(t)$). To second order in the perturbations, we get the single atom correlation terms $\langle \delta Z_j^*(t'_1) \delta Z_j(t'_2) \rangle$ and $\langle \delta XY_j^*(t'_1) \delta XY_j(t'_2) \rangle$. These terms represent the correlations between the atomic positions and velocities at different times. After several collisions with the walls, the atoms lose all memory of their initial position and velocity, and hence for large $|t_1 - t_2|$, the correlations are only through the mean values and all the fluctuations disappear. From now on, we neglect the terms $\propto e^{2ikz_j}$ in Eq. (S29) since these average to zero rapidly. For simplicity, we assume the decay of the correlations to be exponential such that

$$\langle \delta Z_j^*(t'_1) \delta Z_j(t'_2) \rangle = \left(\langle |Z_j|^2 \rangle - |\langle Z_j \rangle|^2 \right) e^{-\Gamma|t'_1 - t'_2|} \quad (\text{S30})$$

$$\langle \delta XY_j^*(t'_1) \delta XY_j(t'_2) \rangle = \left(\langle |XY_j|^2 \rangle - |\langle XY_j \rangle|^2 \right) e^{-\Gamma|t'_1 - t'_2|}, \quad (\text{S31})$$

where Γ is the decay rate of the correlations. We will later justify this assumption by simulating the correlations for a box of non-interacting atoms. In the simulations, we find good agreement with an exponential model with decay rate $\Gamma = \alpha v_{\text{thermal}}/w$, where v_{thermal} is the average thermal velocity of the atoms and α is a numerical constant on the order of unity. Γ is thus given by the average transient time of the atoms through the beam. Employing the exponential decay model, we evaluate the averages, with similar assumptions as before, and arrive at the following expression for $\langle |\theta_j(t)|^2 \rangle$ after performing the integrals and assuming that $e^{-(\kappa_1/2)t} \approx e^{-(\kappa_2/2)t} \approx 0$.

$$\begin{aligned} \langle |\theta_j(t)|^2 \rangle &= |\langle \theta_j(t) \rangle_e|^2 (1 - 2\kappa_1^2 \kappa_2^2 A(\kappa_1, \kappa_2, \Gamma)) + |g|^2 |\Omega|^2 A(\kappa_1, \kappa_2, \Gamma) \\ &\quad \times \left(\frac{\pi^{5/2}}{32 \Gamma_d} \frac{w^4}{L^4} \left(\frac{\text{Re} \{ \mathbf{w}[(\Delta + i\gamma/2)/\Gamma_d] \}}{\gamma/2} + \frac{\text{Im} \{ \mathbf{w}[(\Delta + i\gamma/2)/\Gamma_d] \}}{\Delta} \right) \right. \\ &\quad \left. + \frac{\pi^2}{4 \Gamma_d^2} |w[(\Delta + i\gamma/2)/\Gamma_d]|^2 \frac{w^2}{L^2} \right), \end{aligned} \quad (\text{S32})$$

where we have defined

$$A(\kappa_1, \kappa_2, \Gamma) = \frac{(2\Gamma + \kappa_1 + \kappa_2)}{\kappa_1 \kappa_2 (2\Gamma + \kappa_1)(2\Gamma + \kappa_2)(\kappa_1 + \kappa_2)}. \quad (\text{S33})$$

Using Eqs. (S26) and (S32) we can directly evaluate the write efficiency from Eq. (S18). In the limit of $\kappa_1 \gg (\Gamma, \kappa_2)$ and $\Delta \gg \Gamma_d \gg \gamma$, the expression for η_{write} reduces to Eq. (5) in the article.

Numerical simulation

To justify our assumption of an exponential decay of the correlations appearing in $\langle |\theta_j(t)| \rangle^2$ and to qualitatively characterize the readout efficiency, we perform a numerical simulation of a gas of non-interacting atoms in a cell. We have based the simulation on the microcells filled with Cs-atoms, which are currently being considered for future experiments in our laboratory. These cells have dimensions of $300 \mu\text{m} \times 300 \mu\text{m} \times 1 \text{ cm}$. The cells have been placed inside a cavity with a linewidth of $\kappa_1 \approx 2\pi \cdot 46 \text{ MHz}$ and both the field from the quantum photon and the classical drive are assumed to have approximately a Gaussian shape with a waist of $55 \mu\text{m}$. The small beam waist ensures that we can neglect losses from the walls of the cell. An approximate Λ -atom can be realized in the hyperfine states of Cs with state $|0\rangle = |F=4, m_F=4\rangle$ and state $|1\rangle = |F=3, m_F=3\rangle$ in the $6^2S_{1/2}$ manifold. The Doppler width of the atomic levels is $\Gamma_d \sim 2\pi \cdot 225 \text{ MHz}$ at a temperature of $T = 293 \text{ K}$ and we assume a detuning of $\Delta \sim 4\Gamma_d$ from the excited level such that the effect of Doppler broadening is negligible (see below).

The starting point of our simulations is Eq. (S27) but we do not make the assumption of $k_c \approx k_q \approx k$, as in our analytical calculations, since we have the $2\pi \cdot 9.2 \text{ GHz}$ splitting between the ground states, which corresponds to $k_q - k_c = \Delta_k \approx 193 \text{ m}^{-1}$. As a result, the expression for $Z_j(t)$ is

$$Z_j(t) = \frac{e^{i(\Delta_k)z_j(t)} - e^{-i(k_c+k_q)z_j(t)}}{-\gamma/2 + i(\Delta + k_c v_z^{(j)}(t))} + \frac{e^{-i(\Delta_k)z_j(t)} - e^{i(k_c+k_q)z_j(t)}}{-\gamma/2 + i(\Delta - k_c v_z^{(j)}(t))}, \quad (\text{S34})$$

which reduces to Eq. (S29) for $\Delta_k = 0$. The extra terms $\propto e^{\pm i\Delta_k z_j}$ will approximately result in a factor of

$$c_{\Delta k} = \frac{\langle \cos(\Delta_k z_j) \rangle^2}{\langle \cos(\Delta_k z_j)^2 \rangle}, \quad (\text{S35})$$

which should be multiplied with the analytical expression for the write efficiency, which was obtained assuming $\Delta_k = 0$. Fig. S4 shows how $c_{\Delta k}$ depends on the length of the cell assuming that the atoms are equally distributed in the entire cell. It is seen from Fig. S4 that as long as the length of the cell is $2L_z \lesssim 1 \text{ cm}$ then $c_{\Delta k} \gtrsim 0.97$ for $\Delta_k \approx 193 \text{ m}^{-1}$ and hence the frequency difference between the quantum and classical fields does not significantly degrade the write efficiency. In all our numerical simulations, we, however, keep the terms $\propto e^{\pm i\Delta_k z_j}$ for completeness.

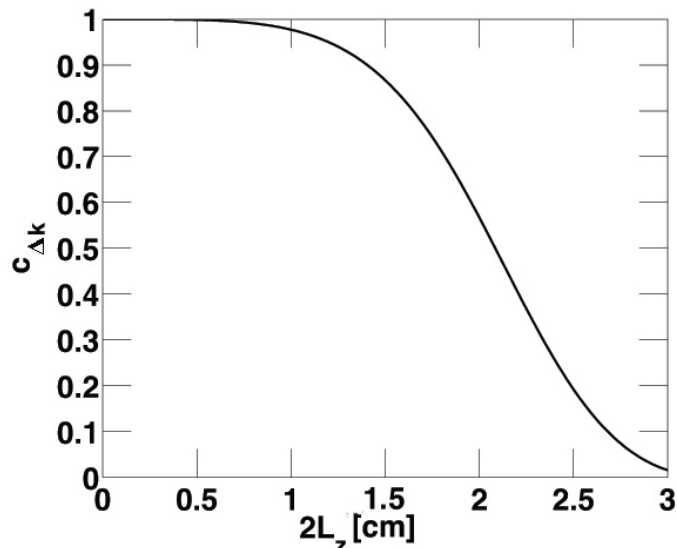


FIG. S4. Limitation in efficiency, $c_{\Delta k}$, from different wavenumbers as a function of the cell length $2L_z$ for $\Delta_k \approx 193 \text{ m}^{-1}$ corresponding to the $2\pi \cdot 9.2 \text{ GHz}$ splitting between the hyperfine ground states of ^{133}Cs . The atoms are assumed to be evenly distributed in the cell. $c_{\Delta k} \gtrsim 0.97$ for $2L_z \lesssim 1 \text{ cm}$.

The correlations appearing in $\langle XY_j^*(t_1'')XY_j(t_2'')Z_j^*(t_1'')Z_j(t_2'') \rangle_e$ (see Eq. (S27)) depend on $|t_1'' - t_2''|$ and we therefore introduce the shorthand notation $\langle XY_j^*(t_1'')XY_j(t_2'')Z_j^*(t_1'')Z_j(t_2'') \rangle_e = \langle XY, Z \rangle_e(t_1'' - t_2'')$. We change to the variables $u = t_1'' + t_2''$ and $s = t_1'' - t_2''$ and by changing the order of integration, we can perform the integrals over t, t_1', t_2' and u . To obtain the write efficiency η_{write} , we need to perform an additional integration over t (see Eq. (S18)). We are therefore left with

$$\int_0^{t_{\text{int}}} \langle |\theta(t)|^2 \rangle_e dt = \int_0^{t_{\text{int}}} h(t_{\text{int}}, \kappa_1, \kappa_2, s) \langle XY, Z \rangle_e(s) ds, \quad (\text{S36})$$

where $h(t_{\text{int}}, \kappa_1, \kappa_2, s)$ is a function of s obtained by performing the integrals over t, t_1', t_2' and u . We can evaluate the integral over s numerically by simulating the correlations $\langle XY, Z \rangle_e(s)$. Since the atoms do not interact with each other, we independently simulate the motion of $N = 5000$ atoms through the cell and evaluate the correlations of atoms at points separated in time by s . Finally, we average over many realizations. The atoms are assumed to be evenly distributed in the cell and their velocity distribution is assumed to follow a Maxwell Boltzmann distribution at a temperature $T = 293 \text{ K}$. We assume that the atoms are rethermalized completely after every collision with the walls of the cell but qualitatively similar results are obtained for a ballistic model without thermalization. For the ballistic model, the Z_j parts of the couplings in principle do not average down and Eq. (S30) is no longer strictly valid. In principle, this could lead to effects not averaged away by using narrow filter cavities. However, we are far detuned compared to the Doppler width of the atoms and the cavity fields are standing waves, which can be viewed as the superposition of two counter propagating waves. As a result, the effect of the velocity fluctuations of the atoms cancel and the fluctuations in the Z_j terms are greatly suppressed. This is in contrast to what happens in ensemble based schemes with a laser coming from one side where Doppler effects do not go away by working far off resonance [28]. Consequently, we obtain similar results for the ballistic model as for the model with complete thermalization. The result of a simulation with thermalization is seen in Fig. S6a, which shows how the correlations decay as a function of s such that for $s \rightarrow \infty$, we have $\langle XY, Z \rangle_e(s) \rightarrow |\langle XY \rangle_e|^2 |\langle Z \rangle_e|^2$. This enables us to introduce a maximal cutoff, s_{max} , in the numerical integral appearing in Eq. (S36), above which, the correlations have effectively vanished. As a result, we can semianalytically evaluate η_{write} for an arbitrary pulse length t_{int} without additional numerical difficulty. Note that Fig. S6a also shows that the exponential model of the decay of the correlations assumed in our analytical calculations is a good approximation.

Based on our simulations of $\langle XY, Z \rangle_e(t - t')$, we have also estimated the power spectral density, PSD. The PSD was measured in the proof-of-principle experiment (see Fig. 2 in the article) by measuring the Faraday rotation of light transmitted through the cell. In these measurements the light probes a spin component of the atoms perpendicular to an applied magnetic field. As a result the signal is modulated at the Larmor precession frequency. We therefore

consider the modulated power spectral density. We have assumed that

$$\text{PSD}(f) \propto \frac{1}{t_{\text{int}}^2} \int_0^{t_{\text{int}}} dt \int_0^{t_{\text{int}}} dt' \langle XY, Z \rangle_e(t-t') e^{2i\pi f(t-t')} \quad (\text{S37})$$

$$\begin{aligned} &\propto \frac{1}{t_{\text{int}}^2} \int_0^{t_{\text{int}}} dt \int_0^{t_{\text{int}}} dt' |\langle XY \rangle_e|^2 |\langle Z \rangle_e|^2 e^{2i\pi f(t-t')} \\ &\quad + \frac{1}{t_{\text{int}}^2} \int_0^{t_{\text{int}}} dt \int_0^{t_{\text{int}}} dt' (\langle XY, Z \rangle_e(t-t') - |\langle XY \rangle_e|^2 |\langle Z \rangle_e|^2) e^{2i\pi f(t-t')} \end{aligned} \quad (\text{S38})$$

$$\propto \delta_{f,0} + \frac{1}{t_{\text{int}}^2} \int_0^{t_{\text{int}}} dt \int_0^{t_{\text{int}}} dt' (\langle XY, Z \rangle_e(t-t') - |\langle XY \rangle_e|^2 |\langle Z \rangle_e|^2) e^{2i\pi f(t-t')} \quad (\text{S39})$$

where f is the frequency and $\delta_{f,0}$ is the Kronecker delta function. Note that we have assumed that coherent light-atom interaction gives a contribution of $\frac{1}{t_{\text{int}}^2} \int_0^{t_{\text{int}}} dt \int_0^{t_{\text{int}}} dt' |\langle XY \rangle_e|^2 |\langle Z \rangle_e|^2 e^{2i\pi f(t-t')} = \delta(f)$ to the PSD. In the proof-of-principle experiment the atoms are subject to a magnetic field, which makes the atomic spins precess around the mean spin direction with a Larmor frequency of 823.8 kHz. The atomic part of the PSD is thus centered around this frequency. However, the PSD also contains both the shot noise of the light and electronic noise from the measurement equipment. Since we are only interested in the signal from the atomic interaction, we remove this noise by performing a second measurement at a higher Larmor frequency and subtract it from the first measurement. The higher Larmor frequency is chosen such that the two atomic signals are well separated in frequency. The result of this procedure is shown in Fig. S5. The measurement time was 3.3 ms and the data has been binned to get improved statistics. Fig. S5

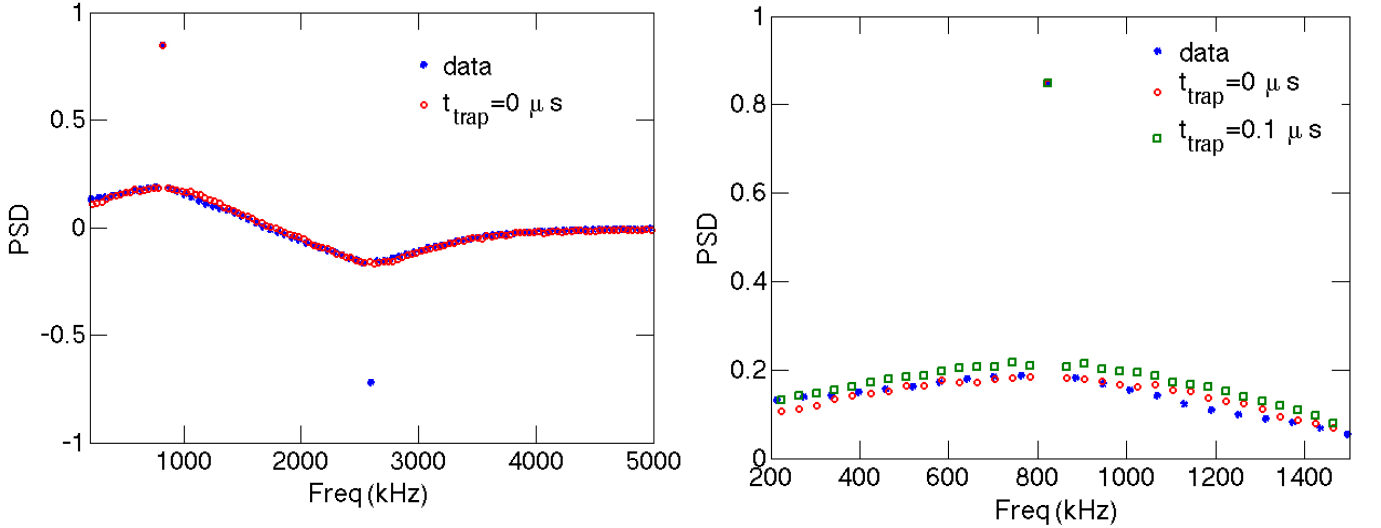


FIG. S5. Measured PSD in the proof-of-principle experiment (data) and simulated SPD for zero trapping time in the coating and a trapping time of $0.1 \mu\text{s}$. The simulations has been rescaled to fit the measured SPD at $f=823.7 \text{ kHz}$. From the figure, we estimate that any trapping time in the experiment is $\lesssim 0.1 \mu\text{s}$ and it can thus be ignored. In the experiment, a cell with dimensions $L = 150 \mu\text{m}$ and $L_z = 1 \text{ cm}$ was used and the light beam had a Gaussian profile with a waist of $w = 55 \mu\text{m}$. The same parameter were used in the simulations. Note that Fig. 2 in the article shows the same measured data and the simulation with zero trapping time for a smaller frequency range.

also shows the simulated SPD, which has been rescaled to correspond to the measured SPD at $f=823.8 \text{ kHz}$. In the simulated SPD, we have fitted a Lorentzian to the broad feature centered at 823.8 kHz and shifted it to be centered at 2594 kHz. This has then been subtracted from simulated data to include the subtraction of the two signals in the experiment. In these simulations, as opposed to our previous simulations, we have also added the possibility of atoms being trapped in the spin-preserving coating of the cells. Nonetheless, Fig. S5 suggests that the trapping time is $t_{\text{trap}} \lesssim 0.1 \mu\text{s}$. Assuming no trapping time, the average return time of an atom that leaves the beam can be estimated to be $\sim 1 \mu\text{s}$. Since $t_{\text{trap}} \ll 1 \mu\text{s}$, it is thus justified to ignore any trapping time in our simulations. The experimental data shown in Fig. S5 agrees nicely with the simulated data thus confirming our theoretical model where atoms can remain coherent even after the atoms leave and return to the beam. This leads to the spectrally narrow peak in the

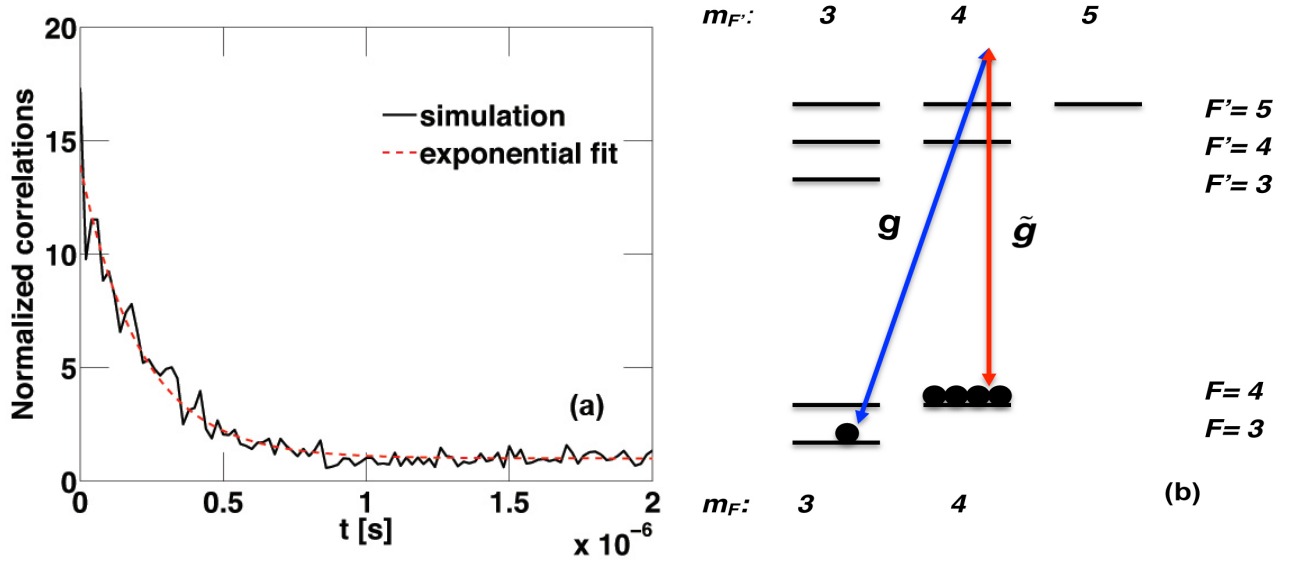


FIG. S6. (a) Simulation of the correlations $\langle XY_j^*(0)XY_j(t)Z_j^*(0)Z_j(t) \rangle_e$. The correlations are normalized to be unity for $t \rightarrow \infty$ where there are no correlations and $\langle XY_j^*(0)XY_j(t)Z_j^*(0)Z_j(t) \rangle_e \rightarrow |\langle XY \rangle_e|^2 |\langle Z \rangle_e|^2$. The data from the simulation have been fitted with an exponential model validating our assumption of an exponential decay of the correlations. The fit gives a decay rate of $\Gamma = 2\pi \cdot 0.75$ MHz corresponding to $\Gamma \sim 1.3v_{\text{thermal}}/w$. (b) Sketch of the $6^2S_{1/2}$ and $6^2P_{3/2}$ hyperfine levels in ^{133}Cs . A Λ -atom is realized with $|0\rangle = |F=4, m_F=4\rangle$, $|1\rangle = |F=3, m_F=3\rangle$ as ground states in $6^2S_{1/2}$ and $|e\rangle = |F'=4, m_{F'=4}\rangle$ as the excited level in $6^2P_{3/2}$. To characterize the optical depth, we consider the transition characterized by \tilde{g} .

spectrum while the broad feature is the incoherent contribution to the signal. The filter-cavity filters out the coherent peak enabling an efficient write process.

NUMBER OF PHOTONS

As mentioned in the article, the purpose of the filter cavity is both to increase the averaging time and to filter the quantum photon from the classical photons. We will now estimate the number of classical photons, which needs to be filtered from the single quantum photon. In order to do this, we need to characterize the ensemble and therefore introduce the optical depth.

To obtain an expression for the optical depth, we assume that we are working with the previously mentioned Cs-cells. The relevant level structure is shown in Fig. S6b. The classical drive (Ω) is applied on the transition characterized by \tilde{g} while the quantum photon is created on the transition characterized by g . Note that with this field configuration, the cell-cavity in principle also mediate the transition $|F=4, m_F=4\rangle \rightarrow |F=4, m_F=3\rangle$ in the write setup but this transition is suppressed by the $2\pi \cdot 9.2$ GHz splitting between the ground states, which makes the corresponding photon non-resonant with the subsequent filter-cavity. This transition will, therefore, never give a click in the detector. Since the interaction is only a perturbation to the system, we can therefore neglect this transition in our numerical simulations. All atoms in the ensemble are initially pumped to the ground state $|0\rangle = |F=4, m_F=4\rangle$ and, in order to characterize the optical depth, we assume that the transition characterized by g is non-driven and ignore any cavity (Purcell) enhancement of the corresponding decay. The cavity field thus only couples $|0\rangle \rightarrow |e_1\rangle$ and $|0\rangle \rightarrow |e_2\rangle$ with coupling constants \tilde{g}_1 and \tilde{g}_2 , respectively. Here $|e_1\rangle = |F'=4, m_{F'}=4\rangle$ and $|e_2\rangle = |F'=5, m_{F'}=4\rangle$ (see Fig. S6b).

The equations of motion for the cavity field, \hat{a}_{cav} , and the relevant atomic operators in a suitable rotating frame are

$$\dot{\hat{a}}_{\text{cav}} = -(\kappa/2)\hat{a}_{\text{cav}} + i \sum_{j=1}^N \left[\tilde{g}_1^{(j)}(t)\hat{\sigma}_{e_1 0}^{(j)} + \tilde{g}_2^{(j)}(t)\hat{\sigma}_{e_2 0}^{(j)} \right] \quad (\text{S40})$$

$$\dot{\hat{\sigma}}_{e_1 0}^{(j)} = -(\gamma_1/2 - i\Delta_1)\hat{\sigma}_{e_1 0}^{(j)} + i\tilde{g}_1^{(j)}(t)\hat{a}_{\text{cav}} \quad (\text{S41})$$

$$\dot{\hat{\sigma}}_{e_2 0}^{(j)} = -(\gamma_2/2 - i\Delta_2)\hat{\sigma}_{e_2 0}^{(j)} + i\tilde{g}_2^{(j)}(t)\hat{a}_{\text{cav}}, \quad (\text{S42})$$

where $\sigma_{e_l 0}^{(j)} = |e_l\rangle_j \langle 0|$ ($l = 1, 2$) and we have assumed that $\sigma_{e_l e_l}^{(j)} - \sigma_{00}^{(j)} \approx -1$. For simplicity, we have assumed the couplings (\tilde{g}) to be real. $\Delta_1 = \omega_1 - \omega_{\text{cav}}$ ($\Delta_2 = \omega_2 - \omega_{\text{cav}}$) is the detuning of $|e_1\rangle$ ($|e_2\rangle$), while γ_1 (γ_2) is the corresponding decay rate. Here ω_1 (ω_2) is the frequency associated with the atomic level and ω_{cav} is the frequency of the cavity field. Formally integrating Eqs. (S41)-(S42), assuming that $\sigma_{e_1 0}^{(j)} = \sigma_{e_2 0}^{(j)} = 0$ at time $t = 0$, and inserting the resulting expression for $\sigma_{e_1 0}^{(j)}$ and $\sigma_{e_2 0}^{(j)}$ into Eq. (S40) gives

$$\begin{aligned} \dot{\hat{a}}_{\text{cav}} = & -(\kappa/2)\hat{a}_{\text{cav}} - \sum_{j=1}^N \left[\tilde{g}_1^{(j)}(t) \int_0^t e^{-(\gamma_1 - i\Delta_1)(t-t')} \tilde{g}_1^{(j)}(t') \hat{a}_{\text{cav}}(t') dt' \right. \\ & \left. + \tilde{g}_2^{(j)}(t') \int_0^t e^{-(\gamma_2 - i\Delta_2)(t-t')} \tilde{g}_2^{(j)}(t') \hat{a}_{\text{cav}}(t') dt' \right], \end{aligned} \quad (\text{S43})$$

where we have explicitly written the time dependence of \hat{a}_{cav} inside the integrals. We evaluate the integrals in Eq. (S43) assuming that we can treat $\hat{a}_{\text{cav}}(t')$ as a constant in time and move it outside the integrals. Furthermore, we assume that $\tilde{g}_l^{(j)}(t') = \tilde{g}_{l,xy}^{(j)}(t) \sin(k(z_j(0) + v_z^{(j)}(0)t'))$ similar to the procedure described in Eq. (S19) and below. Note that k is the wavenumber associated with the cavity field while $z_j(0)$ ($v_z^{(j)}$) is the z -part of the position (velocity) of the j 'th atom. After evaluating the integrals, we obtain

$$\dot{\hat{a}}_{\text{cav}} = -(\kappa/2)\hat{a}_{\text{cav}} + \frac{\hat{a}_{\text{cav}}}{4} \sum_{j=1}^N \left[\left| \tilde{g}_{1,xy}^{(j)}(t) \right|^2 Z_j(\Delta_1, \gamma_1, k) + \left| \tilde{g}_{2,xy}^{(j)}(t) \right|^2 Z_j(\Delta_2, \gamma_2, k) \right], \quad (\text{S44})$$

where we have adiabatically eliminated the decay of the atoms and have rewritten $Z_j(t)$ defined in Eq. (S29) to

$$Z_j(\Delta, \gamma, k) = \frac{e^{2ikz_j(t)} - 1}{\gamma/2 + i(kv_j(0) - \Delta)} - \frac{1 - e^{-2ikz_j(t)}}{\gamma/2 - i(kv_j(0) + \Delta)}, \quad (\text{S45})$$

such that γ, Δ , and k become variable parameters. We now perform an ensemble average of Eq. (S44) assuming that the atoms are evenly distributed in the cell and that their velocity distribution follows a Maxwell Boltzmann distribution, as previously considered. Furthermore, we assume that the xy -dependence of the couplings are Gaussians similar to Eq. (S22) and that we are detuned far from the Doppler width of the atoms. This results in

$$\dot{\hat{a}}_{\text{cav}} = -(\kappa/2)\hat{a}_{\text{cell}} - \frac{\hat{a}_{\text{cell}} N}{4} \left[\frac{|\tilde{g}_1|^2 \gamma_1}{\gamma_1^2/4 + \Delta_1^2} + \frac{|\tilde{g}_2|^2 \gamma_2}{\gamma_2^2/4 + \Delta_2^2} \right] \frac{\pi w^2}{8 L^2} + i[\dots], \quad (\text{S46})$$

where the imaginary part is contained in $[\dots]$. The second term in Eq. (S46) is identified as the single pass optical depth, \tilde{d} , divided by the cavity round trip time, τ , where $\exp(-\tilde{d})$ is the attenuation of the light field after passing through the ensemble. Since \tilde{d} depends on, e.g., the detuning, it is not a direct characterisation of the ensemble. Instead, in analogy with Ref. [29], we characterise the ensemble by d , the hypothetical optical depth, which would be obtained for resonant fields in the absence of Doppler broadening and hyperfine interaction, i.e., Eq. (S46) with $\Delta_1 = \Delta_2 = 0$. Furthermore, we assume that $\gamma_1 = \gamma_2 = \gamma$ such that the optical depth is

$$d = \frac{N\tau}{\gamma} \left(|\tilde{g}_1|^2 + |\tilde{g}_2|^2 \right) \alpha_{xy} \quad (\text{S47})$$

where we have defined the factor $\alpha_{xy} = \frac{\pi w^2}{8 L^2}$. Note that Eq. (S47) can be rewritten to the following well known formula for the optical depth [30]

$$d = 6\pi \frac{N}{(2L)^2} \tilde{\lambda}^2 \left(\frac{\gamma_1 + \gamma_2}{\gamma} \right), \quad (\text{S48})$$

where $2L$ is the transverse size of the cell, $\tilde{\lambda} = \lambda/2\pi$ is the rescaled wavelength of the light, and γ_s is the spontaneous decay rate of level e_s back to $|0\rangle$ ($s=1,2$). The optical depth can also be related to the Faraday rotation angle, θ_F , which is typically measured in experiments and used to estimate the number of atoms, N in the ensemble [13, 31]. For ^{133}Cs , the relation between θ_F and N is [31]

$$N = \left| \frac{32\pi L^2 \theta_F \Delta_2}{a_1(\Delta_2) \gamma \lambda^2} \right| \quad (\text{S49})$$

where $a_1(\Delta_2)$ is the vector polarizability given by

$$a_1(\Delta_2) = \frac{1}{120} \left(-\frac{35}{1 - \Delta_{3'5'}/\Delta_2} - \frac{21}{1 - \Delta_{4'5'}/\Delta_2} + 176 \right), \quad (\text{S50})$$

with $\Delta_{x'5'}$ denoting the hyperfine splitting between level $F' = x$ and $F' = 5$. Combining Eq. (S48) and Eq. (S49) gives the following relation between d and θ_F

$$d = \left| \frac{12\Delta_2\theta_F}{a_1(\Delta_2)} \frac{\gamma_1 + \gamma_2}{\gamma^2} \right| \quad (\text{S51})$$

For the cells considered for future experiments, the Faraday rotation angle has been measured to be 4.4° for a detuning of $\Delta = 2\pi \cdot 850$ MHz. This translates into an optical depth of $d \approx 84$.

Having defined the optical depth, we can now estimate the number of classical photons that need to be filtered from the quantum photon. The field at the detector (see Fig. 1b in the article) is described by the operator \hat{a} in Eq. (S15). Assuming a length, t_{int} , of the write pulse, we estimate the average number of quantum photons, N_{quant} at the detector as

$$N_{\text{quant}} = \langle \hat{a}^\dagger \hat{a} \cdot t_{\text{int}} \rangle = \frac{1}{16} \kappa_2^2 \kappa_1 N \langle |\theta_j|^2 \rangle_e, \quad (\text{S52})$$

where we have used that $\langle |\theta_j|^2 \rangle_e$ is independent of time as shown in Eq. (S32). Note that $\langle |\theta_j|^2 \rangle_e \propto |g|^2 |\Omega|^2$ and we estimate the number of classical photons contained in the write pulse as $N_{\text{clas}} \sim |\Omega|^2 t_{\text{int}} \kappa_1 / (4|\tilde{g}|^2) = |\Omega|^2 t_{\text{int}} \kappa_1 / (4\beta |g|^2)$, where $\beta = |\mu_{\tilde{g}}|^2 / |\mu_g|^2$ is the ratio between the Clebsh-Gordan coefficients (μ) of the transitions characterized by \tilde{g} and g (see Fig. S6b). From Eq. (S52), we then get

$$N_{\text{clas}} \sim \frac{N_{\text{quant}}}{N} \frac{4}{|g|^4 \langle |\theta|^2 \rangle \beta \kappa_2^2}. \quad (\text{S53})$$

The number of classical photons that needs to be filtered is finally estimated by setting $N_{\text{quant}} = 1$. Using Eqs. (S47)-(S48), we can express N_{clas} in terms of the optical depth and the finesse of the cell-cavity, defined as $\mathcal{F} = 2\pi/(\tau\kappa_1)$, where τ is the cavity roundtrip time. Furthermore, we assume that $\langle |\theta_j|^2 \rangle_e \approx |\langle \theta_j \rangle_e|^2$ such that the number of classical photons can be estimated as

$$N_{\text{clas}} \sim \frac{8\pi\beta_2^2 L^2 \Delta^2}{3\beta \tilde{\lambda}^2 \gamma (\gamma_1 + \gamma_2)} \frac{1}{d\mathcal{F}^2}, \quad (\text{S54})$$

where we have expanded the expression for $|\langle \theta_j \rangle|^2$ in the limit of large detuning. $\beta_2 = \frac{|\mu_{g1}|^2 + |\mu_{g2}|^2}{|\mu_g|^2}$ is the ratio between the Clebsh-Gordan coefficients of the transitions characterized by \tilde{g}_1, \tilde{g}_2 and g in Fig. S6b. For the experimental Cs-cells and a detuning of $\Delta = 2\pi \cdot 898$ MHz, we find that $N_{\text{clas}} \sim \frac{7.4 \cdot 10^{11}}{d\mathcal{F}^2}$. With $d = 84$ and $\mathcal{F} = 100$ this gives $N_{\text{clas}} = 9 \cdot 10^5$. Since the quantum and classical field differ both in polarisation and frequency this level of filtering is expected to be easily obtained using both polarization filtering and the filter-cavity.

READOUT

In this section, we go through the details of the readout process. As for the analytical treatment of the write process, we will, for now, assume that the atoms are perfect Λ -atoms. We will later include the complex level structure of ^{133}Cs in a numerical treatment of the readout efficiency. The interaction between the atoms and the light is described by the Hamiltonian

$$\hat{H}_{\text{read}} = - \sum_{j=1}^N \Delta \hat{\sigma}_{ee}^{(j)} + \left(\frac{\Omega_j(t)}{2} \hat{\sigma}_{e1}^{(j)} + g_j(t) \hat{a}_{\text{cell}} \hat{\sigma}_{e0}^{(j)} + H.c. \right), \quad (\text{S55})$$

which is identical to \hat{H}_{write} if $g_j(t)$ and $\Omega_j(t)$ are interchanged (see Eq. (S8)). Including spontaneous emission and cavity decay, as in the write process, we obtain the equations of motion for the cavity field, \hat{a}_{cell} , and the atomic

operators $\hat{\sigma}_{0e}^j$ and $\hat{\sigma}_{01}^j$

$$\frac{d\hat{a}_{\text{cell}}}{dt} = -\frac{\kappa_1}{2}\hat{a} + i \sum_{j=1}^N g_j^*(t) \hat{\sigma}_{0e}^{(j)} \quad (\text{S56})$$

$$\frac{d\hat{\sigma}_{0e}^{(j)}}{dt} = -\left(\frac{\gamma}{2} - i\Delta\right) \hat{\sigma}_{0e}^{(j)} + i g_j(t) \hat{a}_{\text{cell}} + i \frac{\Omega_j(t)}{2} \hat{\sigma}_{01}^{(j)} \quad (\text{S57})$$

$$\frac{d\hat{\sigma}_{01}^{(j)}}{dt} = i \frac{\Omega_j^*(t)}{2} \hat{\sigma}_{0e}^{(j)}, \quad (\text{S58})$$

where we have assumed that $\hat{\sigma}_{ee}^{(j)} - \hat{\sigma}_{00}^{(j)} \approx -\mathbb{I}$ and that the dynamics of $\hat{\sigma}_{10}^{(j)}$ are governed by the classical drive (Ω). Furthermore, we have neglected the noise operators associated with spontaneous emission and cavity decay, as in the write process. We can formally integrate Eq. (S57), assuming the xy -dependence of the couplings to be constant for the integration while the z -dependent parts are of the form $\sin(k(z_j(0) + v_z^{(j)}(0)t))$, as in the write process. Note, that the z -part of the couplings are sinusoidal due to the standing wave in the cavity. Furthermore, we only need to integrate over the motion in the z -direction since the couplings change rapidly with z but vary relatively slowly with x and y due to the broad Gaussian profile of the beams. The integration gives a set of coupled equations

$$\frac{d\hat{a}_{\text{cell}}}{dt} = \mathcal{A}(t) \hat{a}_{\text{cell}} + \sum_{j=1}^N \mathcal{B}_j(t) \hat{\sigma}_{01}^{(j)} \quad (\text{S59})$$

$$\frac{d\hat{\sigma}_{01}^{(j)}}{dt} = \mathcal{B}_j(t) \hat{a}_{\text{cell}} + \mathcal{C}_j(t) \hat{\sigma}_{01}^{(j)}, \quad (\text{S60})$$

where

$$\mathcal{A}(t) = \frac{-\kappa_1}{2} + \frac{1}{4} \sum_{j=1}^N \left| g_{xy}^{(j)}(t) \right|^2 \left(\frac{e^{2ikz_j(t)} - 1}{\gamma/2 - i(\Delta - kv_z^{(j)}(t))} - \frac{1 - e^{-2ikz_j(t)}}{\gamma/2 - i(\Delta + kv_z^{(j)}(t))} \right) \quad (\text{S61})$$

$$\mathcal{B}_j(t) = \frac{1}{8} (g_{xy}^{(j)}(t))^* \Omega_{xy}^{(j)}(t) \left(\frac{e^{2ikz_j(t)} - 1}{\gamma/2 - i(\Delta - kv_z^{(j)}(t))} - \frac{1 - e^{-2ikz_j(t)}}{\gamma/2 - i(\Delta + kv_z^{(j)}(t))} \right) \quad (\text{S62})$$

$$\mathcal{C}_j(t) = \frac{1}{16} \left| \Omega_{xy}^{(j)}(t) \right|^2 \left(\frac{e^{2ikz_j(t)} - 1}{\gamma/2 - i(\Delta - kv_z^{(j)}(t))} - \frac{1 - e^{-2ikz_j(t)}}{\gamma/2 - i(\Delta + kv_z^{(j)}(t))} \right). \quad (\text{S63})$$

We have assumed that $k_c \approx k_q \approx k$ and for simplicity, we have also assumed the couplings (g, Ω) to be real. We now write

$$\mathcal{A}(t) = \langle \mathcal{A}(t) \rangle_e + \delta \mathcal{A}(t) = \bar{\mathcal{A}} + \delta \mathcal{A}(t) \quad (\text{S64})$$

$$\mathcal{B}_j(t) = \langle \mathcal{B}_j(t) \rangle_e + \delta \mathcal{B}_j(t) = \bar{\mathcal{B}} + \delta \mathcal{B}_j(t) \quad (\text{S65})$$

$$\mathcal{C}_j(t) = \langle \mathcal{C}_j(t) \rangle_e + \delta \mathcal{C}_j(t) = \bar{\mathcal{C}} + \delta \mathcal{C}_j(t), \quad (\text{S66})$$

and assume that the couplings consist of large, average and time-independent parts ($\bar{\mathcal{A}}, \bar{\mathcal{B}}, \bar{\mathcal{C}}$) and small, time-dependent perturbations ($\delta \mathcal{A}(t), \delta \mathcal{B}_j(t), \delta \mathcal{C}_j(t)$). Furthermore, we define

$$\hat{S}_l = \frac{1}{\sqrt{N}} \sum_{j=1}^N e^{2i\pi(j-1)l/N} \hat{\sigma}_{01}^{(j)} \quad (\text{S67})$$

$$\mathcal{B}'_l(t) = \frac{1}{\sqrt{N}} \sum_{j=1}^N e^{2i\pi(j-1)l/N} \delta \mathcal{B}_j(t) \quad (\text{S68})$$

$$\mathcal{C}_{l,l'}(t) = \sum_{j=1}^N e^{2i\pi(j-1)(l-l')/N} \delta \mathcal{C}_j(t), \quad (\text{S69})$$

which allows us to transform the system of equations described by Eqs. (S59)-(S60) into

$$\frac{d\mathbf{x}(t)}{dt} = (\mathbf{M}_0 + \delta \mathbf{M}(t)) \mathbf{x}(t), \quad (\text{S70})$$

where $\mathbf{x} = (\hat{a}_{\text{cell}}, \hat{S}_0, \hat{S}_1 \dots \hat{S}_{N-1})$ and

$$\mathbf{M}_0 = \begin{pmatrix} A & \sqrt{N}\bar{\mathcal{B}} & 0 & 0 & \dots & 0 \\ \sqrt{N}\bar{\mathcal{B}} & \bar{\mathcal{C}} & 0 & 0 & \dots & 0 \\ 0 & 0 & \bar{\mathcal{C}} & 0 & \dots & 0 \\ \vdots & \vdots & \vdots & \ddots & & \vdots \\ \vdots & \vdots & \vdots & & \ddots & \vdots \\ 0 & 0 & 0 & \dots & \dots & \bar{\mathcal{C}} \end{pmatrix}, \quad (\text{S71})$$

$$\delta\mathbf{M}(t) = \begin{pmatrix} \delta\mathcal{A}(t) & \mathcal{B}'_0(t) & \mathcal{B}'_{-1}(t) & \mathcal{B}'_{-2}(t) & \dots & \mathcal{B}'_{1-N}(t) \\ \mathcal{B}'_0(t) & \mathcal{C}_{0,0}(t) & \mathcal{C}_{0,1}(t) & \mathcal{C}_{0,2}(t) & \dots & \mathcal{C}_{0,N-1}(t) \\ \mathcal{B}'_1(t) & \mathcal{C}_{1,0}(t) & \mathcal{C}_{1,1}(t) & \mathcal{C}_{1,2}(t) & \dots & \mathcal{C}_{1,N-1}(t) \\ \vdots & \vdots & \vdots & \ddots & & \vdots \\ \vdots & \vdots & \vdots & & \ddots & \vdots \\ \mathcal{B}'_{N-1}(t) & \mathcal{C}_{N-1,0}(t) & \mathcal{C}_{N-1,1}(t) & \dots & \dots & \mathcal{C}_{N-1,N-1}(t) \end{pmatrix}. \quad (\text{S72})$$

With this transformation, we thus keep the mean values in \mathbf{M}_0 , which describes the strongly coupled symmetric mode \hat{S}_0 and the cavity mode \hat{a}_{cell} as well as an overall damping. All fluctuations, on the other hand, are contained in $\delta\mathbf{M}(t)$, which we will treat perturbatively. Assuming that the initial state of the atoms before readout is the symmetric Dicke state, we have that $\hat{S}_{l \neq 0} = 0$ and we find that, to second order in $\delta\mathbf{M}(t)$, the cavity field can be expressed as $\hat{a}_{\text{cell}} \sim \hat{a}_{\text{cell}}^{(0)} + \hat{a}_{\text{cell}}^{(2)}$. Here we have omitted the first order term, which originates from the fluctuations in $\delta\mathcal{A}(t)$ and \mathcal{B}'_0 since we find that they are suppressed by a factor of at least $d\mathcal{F}/N$ compared to the other terms. Here d is the optical depth defined in Eq. (S47) and \mathcal{F} is the finesse of the cell-cavity. The readout efficiency is $\eta_{\text{read}} = \int_0^{\tau_{\text{read}}} dt \kappa_1 \langle \hat{a}_{\text{cell}}^\dagger \hat{a}_{\text{cell}} \rangle$, which to second order is

$$\eta_{\text{read}} \approx \kappa_1 \int_0^{\tau_{\text{read}}} dt \langle (\hat{a}_{\text{cell}}^{(0)}(t))^\dagger \hat{a}_{\text{cell}}^{(0)} \rangle + 2\kappa_1 \text{Real} \left(\int_0^{\tau_{\text{read}}} dt \langle (\hat{a}_{\text{cell}}^{(0)}(t))^\dagger \hat{a}_{\text{cell}}^{(2)} \rangle \right) \quad (\text{S73})$$

$$\approx \eta_{\text{read},0} + \eta_{\text{read},2} \quad (\text{S74})$$

Including only the mean value terms, we find that

$$\begin{aligned} \eta_{\text{read}} &\approx \eta_{\text{read},0} = \kappa_1 \int_0^{\tau_{\text{read}}} dt \langle (\hat{a}_{\text{cell}}^{(0)}(t))^\dagger \hat{a}_{\text{cell}}^{(0)} \rangle \\ &\approx \kappa_1 \int_0^{\tau_{\text{read}}} dt \frac{N |\bar{\mathcal{B}}|^2}{|\mathcal{D}|} e^{\text{Real}(\bar{\mathcal{A}} + \bar{\mathcal{C}})t} \left(e^{\frac{1}{2}\sqrt{\mathcal{D}}t} - e^{-\frac{1}{2}\sqrt{\mathcal{D}}t} \right) \left(e^{\frac{1}{2}\sqrt{\mathcal{D}}^*t} - e^{-\frac{1}{2}\sqrt{\mathcal{D}}^*t} \right), \end{aligned} \quad (\text{S75})$$

where $\mathcal{D} = (\bar{\mathcal{C}} - \bar{\mathcal{A}})^2 + 4N\bar{\mathcal{B}}^2$. In the limit of weak driving and consequently a long readout pulse, Eq. (S75) reduces to Eq. (7) in the article. As mentioned in the article $\eta_{\text{read},0}$ is an upper limit of the readout efficiency. Note that we define the readout rate from Eq. (S75) as $\Gamma_{\text{read}} \approx -\text{Real}(\bar{\mathcal{A}} + \bar{\mathcal{C}} + \sqrt{\mathcal{D}})$.

For the second order term $\eta_{\text{read},2}$ we find

$$\begin{aligned} \eta_{\text{read},2} &= 2\kappa_1 \text{Real} \left(\int_0^{\tau_{\text{read}}} dt \int_0^t dt' \int_0^{t'} dt'' \frac{\sqrt{N}\bar{\mathcal{B}}^*}{2|\mathcal{D}|} e^{\text{Real}(\bar{\mathcal{A}} + \bar{\mathcal{C}})t} \left(e^{\frac{1}{2}\sqrt{\mathcal{D}}^*t} - e^{-\frac{1}{2}\sqrt{\mathcal{D}}^*t} \right) e^{\bar{\mathcal{C}}(t'-t'')} e^{-\frac{1}{2}(\bar{\mathcal{A}} + \bar{\mathcal{C}})(t'-t'')} \right. \\ &\quad \times \left(e^{\frac{1}{2}\sqrt{\mathcal{D}}t} \left(e^{\frac{1}{2}\sqrt{\mathcal{D}}(t'-t'')} - e^{-\frac{1}{2}\sqrt{\mathcal{D}}(t'+t'')} \right) \left(\left[(\bar{\mathcal{A}} - \bar{\mathcal{C}} + \sqrt{\mathcal{D}}) N \langle \delta\mathcal{B}_j(t') \delta\mathcal{B}_j(t'') \rangle_e + 2\bar{\mathcal{B}} N \langle \delta\mathcal{C}_j(t') \delta\mathcal{B}_j(t'') \rangle_e \right] \frac{\sqrt{N}\bar{\mathcal{B}}}{\sqrt{\mathcal{D}}} \right) \right. \\ &\quad + e^{\frac{1}{2}\sqrt{\mathcal{D}}(t+t'-t'')} \left(\left[(\bar{\mathcal{A}} - \bar{\mathcal{C}} + \sqrt{\mathcal{D}}) N \langle \delta\mathcal{B}_j(t') \delta\mathcal{C}_j(t'') \rangle_e + 2\bar{\mathcal{B}}\sqrt{N} \langle \delta\mathcal{C}_j(t') \delta\mathcal{C}_j(t'') \rangle_e \right] \frac{\bar{\mathcal{A}} - \bar{\mathcal{C}} + \sqrt{\mathcal{D}}}{2\sqrt{\mathcal{D}}} \right) \\ &\quad + e^{\frac{1}{2}\sqrt{\mathcal{D}}(t-t'-t'')} \left(\left[(\bar{\mathcal{A}} - \bar{\mathcal{C}} + \sqrt{\mathcal{D}}) N \langle \delta\mathcal{B}_j(t') \delta\mathcal{C}_j(t'') \rangle_e + 2\bar{\mathcal{B}}\sqrt{N} \langle \delta\mathcal{C}_j(t') \delta\mathcal{C}_j(t'') \rangle_e \right] \frac{-\bar{\mathcal{A}} + \bar{\mathcal{C}} + \sqrt{\mathcal{D}}}{2\sqrt{\mathcal{D}}} \right) \\ &\quad \left. + e^{-\frac{1}{2}\sqrt{\mathcal{D}}t} \left(e^{\frac{1}{2}\sqrt{\mathcal{D}}(t'-t'')} - e^{\frac{1}{2}\sqrt{\mathcal{D}}(t'+t'')} \right) \left(\left[(\bar{\mathcal{A}} - \bar{\mathcal{C}} - \sqrt{\mathcal{D}}) N \langle \delta\mathcal{B}_j(t') \delta\mathcal{B}_j(t'') \rangle_e + 2\bar{\mathcal{B}} N \langle \delta\mathcal{C}_j(t') \delta\mathcal{B}_j(t'') \rangle_e \right] \frac{\sqrt{N}\bar{\mathcal{B}}}{\sqrt{\mathcal{D}}} \right) \right) \end{aligned}$$

$$\begin{aligned}
& + e^{\frac{1}{2}\sqrt{\mathcal{D}}(t'+t''-t)} \left(\left[\left(\bar{\mathcal{A}} - \bar{\mathcal{C}} - \sqrt{\mathcal{D}} \right) N \langle \delta \mathcal{B}_j(t') \delta \mathcal{C}_j(t'') \rangle_e + 2\bar{\mathcal{B}}\sqrt{N} \langle \delta \mathcal{C}_j(t') \delta \mathcal{C}_j(t'') \rangle_e \right] \frac{\bar{\mathcal{A}} - \bar{\mathcal{C}} - \sqrt{\mathcal{D}}}{2\sqrt{\mathcal{D}}} \right) \\
& + e^{\frac{1}{2}\sqrt{\mathcal{D}}(t'-t''-t)} \left(\left[\left(\bar{\mathcal{A}} - \bar{\mathcal{C}} - \sqrt{\mathcal{D}} \right) N \langle \delta \mathcal{B}_j(t') \delta \mathcal{C}_j(t'') \rangle_e + 2\bar{\mathcal{B}}\sqrt{N} \langle \delta \mathcal{C}_j(t') \delta \mathcal{C}_j(t'') \rangle_e \right] \frac{\bar{\mathcal{A}} + \bar{\mathcal{C}} - \sqrt{\mathcal{D}}}{2\sqrt{\mathcal{D}}} \right) \Bigg) \Bigg). \quad (\text{S76})
\end{aligned}$$

Here we have, once again, neglected the contributions from the fluctuations contained in $\delta \mathcal{A}(t)$ and \mathcal{B}_0 since they are suppressed by a factor of at least $d\mathcal{F}/N$ compared to the terms above. In deriving Eq. (S76), we have used that $\hat{a}_{\text{cell}}^{(2)}$ consists of sums of the form

$$\frac{1}{N} \sum_{l=1}^{N-1} \sum_{j=1}^N \sum_{j'=1}^N e^{-2i\pi/N(j-j')l} \delta X_j(t') \delta X_{j'}(t''), \quad (\text{S77})$$

where X_j could e.g. denote \mathcal{B}_j . For $\eta_{\text{read},2}$, we calculate $\langle \hat{a}_{\text{cell}}^{(0)} \hat{a}_{\text{cell}}^{(2)} \rangle$ and the average of Eq. (S77) is approximately $N \langle \delta X_j(t') \delta X_j(t'') \rangle_e$ because $\langle \delta X_j(t') \delta X_{j'}(t'') \rangle = 0$, if $j \neq j'$, since the motion of different atoms are uncorrelated and we have assumed that $N-1 \approx N$. All correlations appearing in Eq. (S76) are thus single atom correlations and the index j is kept to indicate this. The correlations contained in $\eta_{\text{read},2}$ can be treated analytically, in a similar fashion as the correlations in $\langle |\theta_j(t)|^2 \rangle$ for the write process, but we have, however, treated the correlations numerically by simulating the previously mentioned Cs-cells.

Numerical simulation

The simulations are performed in the same way as for the write process. An extra difficulty is, however, that we consider the coupling between the light fields and the extra levels in ^{133}Cs . We assume that the readout process has the level structure shown in Fig. S7.

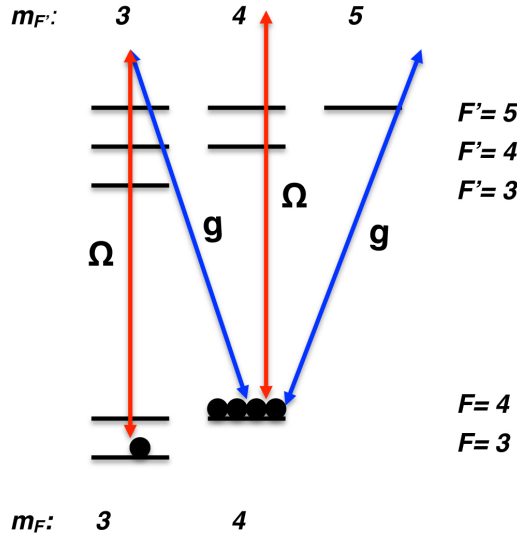


FIG. S7. Schematic view of the readout realized in the hyperfine levels of $6^2S_{1/2}$ and $6^2P_{3/2}$ in ^{133}Cs . We imagine the single excitation to be stored in state $|F=3, m_F=3\rangle$ while the macroscopically populated state is $|F=4, m_F=4\rangle$. Note that the classical drive also couples $|F=4, m_F=4\rangle$ to $|F'=4, m_{F'}=4\rangle$ and $|F'=5, m_{F'}=4\rangle$, which can pump atoms out of the ground state. These couplings are however sufficiently suppressed by the large splitting of $2\pi \cdot 9.2$ GHz between the ground states.

The couplings to the extra levels result in extra coupling terms in the expressions for \mathcal{A} , \mathcal{B}_j and \mathcal{C}_j , which we include, but the expression for $\eta_{\text{read},2}$ is still the same as given in Eq. (S76). Note, however, that a cavity detuning of the quantum field (appearing in the expression for \mathcal{A}) is needed to compensate the phases resulting from some of these additional couplings. The starting point of our numerical simulations is therefore Eq. (S76), where we can change the

order of integration and introduce the variables $u = t' + t''$ and $s = t' - t''$ since the correlations only depend on the time difference $|t' - t''|$. Performing the integrals over t and u analytically, allows us to write

$$\eta_{\text{read},2} = \int_0^{\tau_{\text{read}}} (h_1(\tau_{\text{read}}, s) \langle \delta \mathcal{B}, \delta \mathcal{B} \rangle_e(s) + h_2(\tau_{\text{read}}, s) \langle \delta \mathcal{B}, \delta \mathcal{C} \rangle_e(s) + h_3(\tau_{\text{read}}, s) \langle \delta \mathcal{C}, \delta \mathcal{B} \rangle_e(s) + h_4(\tau_{\text{read}}, s) \langle \delta \mathcal{C}, \delta \mathcal{C} \rangle_e(s)) ds, \quad (\text{S78})$$

where $h_1(\tau_{\text{read}}, s)$, $h_2(\tau_{\text{read}}, s)$, $h_3(\tau_{\text{read}}, s)$ and $h_4(\tau_{\text{read}}, s)$ are functions of s and τ_{read} , which are obtained from the integration over t and u . We have once again introduced the short notation for the correlations $\langle \delta \mathcal{B}_j(t') \delta \mathcal{C}_j(t'') \rangle_e = \langle \delta \mathcal{B}, \delta \mathcal{C} \rangle_e(s)$. Note that $\langle \delta \mathcal{B}, \delta \mathcal{C} \rangle_e(s) \rightarrow 0$ for $s \rightarrow \infty$ similar to the situation in the write process, i.e., the coupling of an atom at time t is uncorrelated from its initial coupling if t is large. We can therefore introduce a cutoff s_{max} in the integral in Eq. (S78) such that we can evaluate $\eta_{\text{read},2}$ for an arbitrary length of the readout pulse τ_{read} without additional numerical difficulty. We then numerically evaluate $\eta_{\text{read},2}$ from Eq. (S78) by simulating the decay of the correlations similar to the simulation of the write process. From the numerical simulation, we find that the term $\langle \delta \mathcal{C}_j \delta \mathcal{C}_j \rangle_e$ dominates $\eta_{\text{read},2}$. This term describes loss of the excitation due to spontaneous emission to modes not confined by the cavity.

ERRORS

We will now consider the various errors and imperfections, which limit the performance of a DLCZ repeater based on the system considered in our work. The write efficiency, η_{write} , as defined in Eq. (S17) can also be viewed as the conditional fidelity of the atomic state with the symmetric Dicke state following a click in the detector. In the entanglement setup of a DLCZ repeater, two ensembles are driven weakly and any emitted quantum photons are sent to a central balanced beam splitter and subsequently detected. If the excitation probability is small, the detection of a photon, to good approximation, heralds a Bell-type state between the two ensembles, where the single excitation is shared between them. In such a setup, the write efficiency would translate into an error in the fidelity of the entangled state. However, a write efficiency of 90% means that the atomic state basically contains a mixture of 10% vacuum, which can never subsequently produce a photon upon readout. The entanglement swap in a DLCZ repeater relies on reading out the stored excitation and the vacuum part would therefore not result in a detection event. Hence, the error from the write process is converted into a total efficiency of $\eta_{\text{write}} \eta_{\text{read}}$. Inefficient motional averaging in the write process thus degrades the efficiency but not the fidelity. The same argument applies if a single ensemble is simply used as a single photon source.

In order to create a single excitation in the write process, we have assumed that the ensemble is driven weakly. There is, however, always a finite probability of creating multiple excitations in the ensemble during the write process, which can introduce an error in the fidelity of the entanglement setup in a DLCZ repeater. Multiple excitations would also create multiple quantum photons, which could in principle be discriminated from the situation with a single quantum photon using perfect number resolving detectors and assuming that no photons were lost between the cavity and the detectors. However, assuming number resolving detectors, but finite detection probability, η_d , the multiple excitations will introduce an error of $\sim 2(1 - \eta_d)\epsilon$ to lowest order where $\epsilon \propto \int_0^{t_{\text{int}}} \langle |\theta_j(t)|^2 \rangle$ is the excitation probability. This error can be made arbitrarily small by simply decreasing α , i.e. decreasing the strength of the classical drive. This will, however, also decrease the success probability of the entangling process and hence, the rate of entanglement creation.

There are a number of errors, which cannot simply be described as inefficiencies. The photons being read out from two ensembles should be coherent, i.e. they should be indistinguishable. Any incoherence will e.g. translate into an error in the average fidelity in a DLCZ protocol. During the readout process, the excitation may not be read out collectively but rather as a single atom readout. As a result, the photon will have a random phase depending on which atom was read out, which degrades the coherence when using the ensemble as a single photon source. We characterize the error from this process by considering a Hong-Ou-Mandel experiment [32]. We assume, that we have successfully stored two single excitations in two ensembles. The excitations are read out simultaneously and combined on a balanced beam splitter. Each output port of the beamsplitter is detected with a single photon detector. If indistinguishable photons are incident on the beam splitter, they will bunch together and only one of the output detectors will give a click. If, however, they are distinguishable, there is a 50 % probability that both detectors clicks. Letting \hat{a} (\hat{b}) characterize the photon from ensemble one (two), we can write the probability of a click in both detectors

as

$$\epsilon_c = \frac{1}{2\eta_{\text{read}}^2} \int_0^\infty dt \int_0^\infty dt' \left\langle (\hat{a}(t))^\dagger (\hat{b}(t'))^\dagger \hat{b}(t') \hat{a}(t) + (\hat{a}(t'))^\dagger (\hat{b}(t))^\dagger \hat{b}(t) \hat{a}(t') \right. \\ \left. - (\hat{a}(t))^\dagger (\hat{b}(t'))^\dagger \hat{b}(t) \hat{a}(t') - (\hat{a}(t'))^\dagger (\hat{b}(t))^\dagger \hat{b}(t') \hat{a}(t) \right\rangle, \quad (\text{S79})$$

where the factor of $1/(2\eta_{\text{read}}^2)$ ensures correct normalization (η_{read} is the total readout efficiency) such that for perfectly coherent photons $\epsilon_c = 0$ while for completely distinguishable photons, $\epsilon_c = 1$. From our perturbative calculation of the readout efficiency, we have that, $\hat{a} \sim \hat{a}^{(0)} + \hat{a}^{(2)}$ and $\hat{b} \sim \hat{b}^{(0)} + \hat{b}^{(2)}$ to second order, assuming that single symmetric excitations were stored in both ensembles. Inserting these expressions into Eq. (S79) gives, to second order in $\hat{a}^{(2)}$ and $\hat{b}^{(2)}$,

$$\epsilon_c^{(2)} = \frac{1}{\eta_{\text{read}}^2} \int_0^\infty dt \int_0^\infty dt' \left\langle 2(\hat{a}^{(2)}(t))^\dagger (\hat{b}^{(0)}(t'))^\dagger \hat{b}^{(0)}(t') \hat{a}^{(2)}(t) + (\hat{a}^{(2)}(t'))^\dagger (\hat{b}^{(0)}(t))^\dagger \hat{b}^{(2)}(t) \hat{a}^{(0)}(t') \right. \\ \left. - 2(\hat{a}^{(2)}(t))^\dagger (\hat{b}^{(0)}(t'))^\dagger \hat{b}^{(2)}(t) \hat{a}^{(0)}(t') - (\hat{a}^{(2)}(t'))^\dagger (\hat{b}^{(0)}(t))^\dagger \hat{b}^{(0)}(t') \hat{a}^{(2)}(t) \right\rangle, \quad (\text{S80})$$

where we have used that e.g. $\langle (\hat{a}^{(2)}(t))^\dagger (\hat{b}^{(0)}(t'))^\dagger \hat{b}^{(0)}(t') \hat{a}^{(2)}(t) \rangle = \langle (\hat{a}^{(0)}(t'))^\dagger (\hat{b}^{(2)}(t))^\dagger \hat{b}^{(2)}(t) \hat{a}^{(0)}(t') \rangle$ since the two setups are identical. The expression for $\hat{a}^{(0)}$ ($\hat{b}^{(0)}$) and $\hat{a}^{(2)}$ ($\hat{b}^{(2)}$) are found from Eqs. (S75)-(S76). Note, that while $\eta_{\text{read},2}$ contains two-point correlations of the form $\langle \delta \mathcal{B}_j(t) \delta \mathcal{B}_j(t') \rangle$, we find that these cancel in Eq. (S80) and we are left with four-point correlations of the form $\langle \delta \mathcal{B}_j(t) \delta \mathcal{B}_j(t') \delta \mathcal{B}_j(t'') \delta \mathcal{B}_j(t''') \rangle$. These are suppressed by a factor of $1/N$ compared to the two-point correlations and since $N \gg 1$ ($N \sim 10^7$ in the Cs-cells that we consider), the error from $\epsilon_c^{(2)}$ can be neglected compared to e.g. the error from assymmetric excitations discussed below.

Another source of incoherence originates from inefficient optical pumping and scattering of atoms through spontaneous emission during the write process. Both of these processes result in excitations being stored in assymmetric modes described by the operators $\hat{S}_{l \neq 0}$ (see Eq. (S67)), which upon readout can degrade the coherence of the photons. The contribution to the single photon field from these assymmetric modes can be found from our perturbative treatment of \hat{a}_{cell} in the readout process. Letting p_{pump} denote the probability of a single atom being in the $|1\rangle$ state instead of $|0\rangle$, the average excitation of the assymmetric mode is p_{pump} . Note, that the dominant process, taking a single atom to state $|1\rangle$, will be inefficient optical pumping for realistic systems. We find that the assymmetric modes gives a first order contribution of

$$\hat{a}^{(1)}(t) = \sqrt{\kappa_1 p_{\text{pump}}} \int_0^t dt' \frac{e^{\frac{1}{2}(\bar{\mathcal{A}} + \bar{\mathcal{C}})(t-t')}}{2\sqrt{\mathcal{D}}} e^{\bar{\mathcal{C}}t'} \frac{1}{\sqrt{N}} \sum_{l=1}^{N-1} \sum_{j=1}^N e^{-2i\pi(j-1)l/N} \left(\left(e^{\frac{1}{2}\sqrt{\mathcal{D}}(t-t')} - e^{-\frac{1}{2}\sqrt{\mathcal{D}}(t-t')} \right) ((\bar{\mathcal{A}} - \bar{\mathcal{C}}) \delta \mathcal{B}_j(t') + 2\bar{\mathcal{B}} \delta \mathcal{C}_j(t')) \hat{S}_l \right. \\ \left. + \left(e^{\frac{1}{2}\sqrt{\mathcal{D}}(t-t')} + e^{-\frac{1}{2}\sqrt{\mathcal{D}}(t-t')} \right) \sqrt{\mathcal{D}} \delta \mathcal{B}_j(t') \hat{S}_l \right). \quad (\text{S81})$$

where κ_1 is the decay rate of the cavity. Employing the Hong-Ou-Mandel analysis described above, we find that the resulting incoherence to lowest order is

$$\epsilon_c^{(1)} = \frac{1}{\eta_{\text{read}}^2} \int_0^\infty dt \int_0^\infty dt' \left\langle 2(\hat{a}^{(1)}(t))^\dagger (\hat{b}^{(0)}(t'))^\dagger \hat{b}^{(0)}(t') \hat{a}^{(1)}(t) \right. \\ \left. - (\hat{a}^{(1)}(t'))^\dagger (\hat{b}^{(0)}(t))^\dagger \hat{b}^{(0)}(t') \hat{a}^{(1)}(t) \right\rangle. \quad (\text{S82})$$

We can numerically evaluate the correlations contained in Eq. (S82) in a similar fashion as the correlations in $\eta_{\text{read},2}$, i.e., we simulate the experimental Cs-cells. We find that the second term in Eq. (S82) can be neglected since the readout rate of the assymmetric excitation described by $\hat{a}^{(1)}$ is much different from the readout rate of the symmetric excitation described by $\hat{a}^{(0)}$. The numerical simulation of $\epsilon_c^{(1)}$ is shown in Fig. S8a where we have assumed that the detectors integrate for a readout time of $\tau_{\text{read}} = 3/\Gamma_{\text{read}}$ where Γ_{read} is the readout rate of the symmetric excitation. The readout time is chosen such that most of the coherent photons are being readout while only a small part of the incoherent photons are being readout.

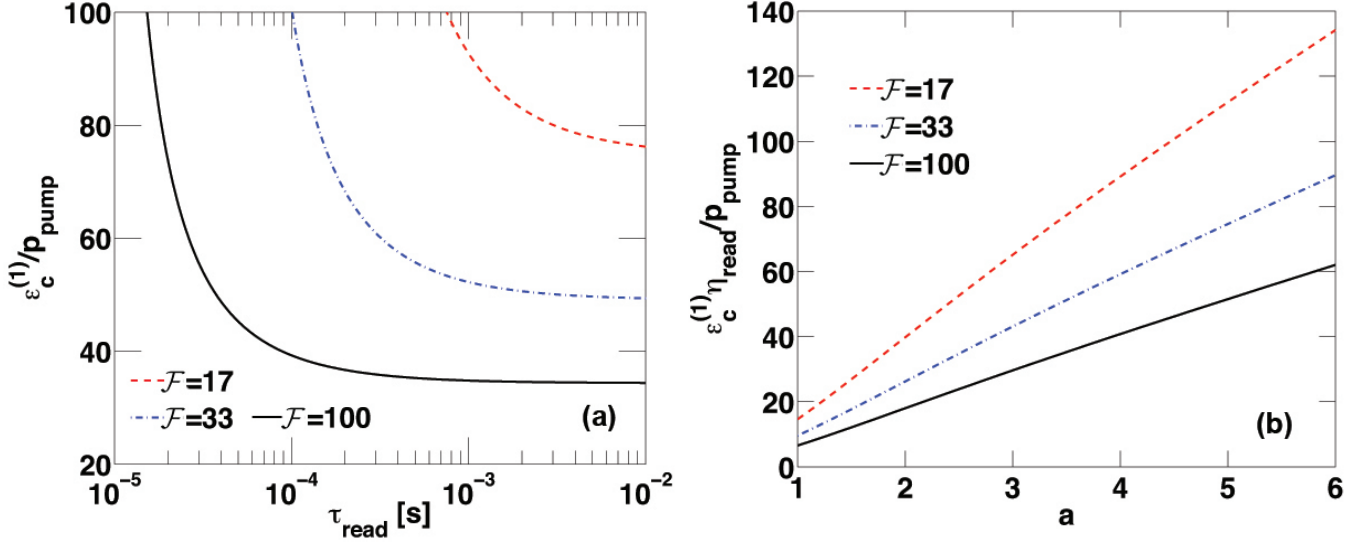


FIG. S8. (a) $\epsilon_c^{(1)}$ plotted against the readout time defined as $\tau_{\text{read}} = 3/\Gamma_{\text{read}}$ where Γ_{read} is the readout rate of the symmetric excitation. (b) $\epsilon_c^{(1)}\eta_{\text{read}}^2/p_{\text{pump}}$ as a function of the parameter a where the readout time is assumed to be $t_{\text{read}} = a/\Gamma_{\text{read}}$. The optical depth is assumed to be 84, as measured in the proof-of-principle experiment. \mathcal{F} is the finesse of the cell-cavity.

From Fig. S8 we find that for a finesse of $\mathcal{F} = 100$ and a readout time of $\approx 180 \mu\text{s}$ for which $\eta_{\text{read}} \approx 90\%$, we have an error of $\epsilon_c^{(1)} \approx 35p_{\text{pump}}$. Assuming that $p_{\text{pump}} = 0.03\%$ we would thus get an error of $\approx 1\%$. The increase in $\epsilon_c^{(1)}$ seen in Fig. S8 for short readout times is because we normalize with $1/\eta_{\text{read}}^2$ (see Eq. (S82)) and η_{read} decreases for short readout times (see Fig. 3b in the article). Parameterizing the readout time as $\tau_{\text{read}} = a/\Gamma_{\text{read}}$ the quantity $\epsilon_c^{(1)}\eta_{\text{read}}^2/p_{\text{pump}}$ effectively only depends on the parameter a for fixed finesse and optical depth. This dependence is shown in Fig. S8b.

For $a \gtrsim 3$, we read out practically all of the coherent photons and it is thus never advantageous to have higher values of a since we are then only reading out more incoherent photons as shown in Fig. S8b.

DLCZ error analysis

In order to fully characterize the performance of a DLCZ repeater based on the room temperature cells, we investigate how the errors from incoherent photons propagates in the repeater. First we consider the state being produced in the entanglement generation step (see above). We define the following parameters:

- η_{write} : The write efficiency, which basically is the probability to have a Dicke state in the ensemble conditioned on a quantum photon being emitted. If we are not in the right state we are dominated by the initial state and thus with probability $1 - \eta_{\text{write}}$, we assume the atomic state to be $|00\dots 0\rangle$.
- ϵ : The excitation probability, which depends on the driving strength.
- P_d : The dark count probability of a detector. We estimate this as $P_d \sim r_{\text{dark}}t_{\text{int}}$ where r_{dark} is the dark count rate and t_{int} is the length of the driving pulse.
- η_d : The detection efficiency, which is determined by the total efficiency of the detector, the outcoupling losses and the transmission losses from the cavity to the detector.

To second order in the excitation probability, the state of the two ensembles following a single click in a detector at the central station is described by the density matrix

$$\begin{aligned}
\rho_{\text{success}} = & \left[\epsilon^2(1 - \eta_{\text{write}})^2(2\eta_d - 2\eta_d^2)(1 - P_d)^2 + 2\epsilon^2(1 - \eta_{\text{write}})^2(1 - \eta_d)^2P_d(1 - P_d) \right. \\
& + 2(1 - \epsilon)^2P_d(1 - P_d) + 4\epsilon(1 - \eta_{\text{write}})(1 - \epsilon)(1 - \eta_d)P_d(1 - P_d) \\
& + 4\epsilon^2(1 - \eta_{\text{write}})^2(\eta_d - \eta_d^2)(1 - P_d)^2 + 4\epsilon^2(1 - \eta_{\text{write}})^2(1 - \eta_d)^2P_d(1 - P_d) \Big] |\mathbf{00}\rangle\langle\mathbf{00}| \\
& + \left[\epsilon^2\eta_{\text{write}}^2(2\eta_d - 2\eta_d^2)(1 - P_d)^2 + 2\epsilon^2\eta_{\text{write}}^2(1 - \eta_d)^2P_d(1 - P_d) \right] |\mathbf{11}\rangle\langle\mathbf{11}| \\
& + \left[\epsilon^2\eta_{\text{write}}(1 - \eta_{\text{write}})(2\eta_d - 2\eta_d^2)(1 - P_d)^2 + 2\epsilon^2\eta_{\text{write}}(1 - \eta_{\text{write}})(1 - \eta_d)^2P_d(1 - P_d) \right. \\
& + 2\epsilon\eta_{\text{write}}(1 - \epsilon)(1 - \eta_d)P_d(1 - P_d) + 4\epsilon^2\eta_{\text{write}}(1 - \eta_{\text{write}})(\eta_d - \eta_d^2)(1 - P_d)^2 \\
& + 4\epsilon^2\eta_{\text{write}}(1 - \eta_{\text{write}})(1 - \eta_d)^2P_d(1 - P_d) \Big] (|\mathbf{01}\rangle\langle\mathbf{01}| + |\mathbf{10}\rangle\langle\mathbf{10}|) \\
& + \left[2\epsilon^2\eta_{\text{write}}^2(\eta_d - \eta_d^2)(1 - P_d)^2 + 2\epsilon^2\eta_{\text{write}}^2(1 - \eta_d)^2P_d(1 - P_d) \right] (|\mathbf{20}\rangle\langle\mathbf{20}| + |\mathbf{02}\rangle\langle\mathbf{02}|) \\
& + 2\epsilon\eta_{\text{write}}(1 - \epsilon)\eta_d(1 - P_d)^2 |\Psi\rangle\langle\Psi| \Big] \frac{1}{\mathcal{N}}, \tag{S83}
\end{aligned}$$

where we have defined $|\mathbf{0}\rangle = |00\dots 0\rangle$, $|\mathbf{1}\rangle = |\text{Dicke}\rangle$, $|\mathbf{2}\rangle = \frac{1}{\sqrt{N}} \sum_{i,j=1}^N |1\rangle_i |1\rangle_j |0\rangle_i |0\rangle_j |00\dots 0\rangle$ and $|\Psi\rangle = \frac{1}{\sqrt{2}}(|\mathbf{01}\rangle + |\mathbf{10}\rangle)$. $\mathcal{N} = P_{\text{success}}$ is a normalization constant, which gives the success probability of the operation. Note that we have assumed number resolving detectors. It is seen from Eq. (S83) that we can write $\rho_{\text{success}} = a_0 |\Psi\rangle\langle\Psi| + b_0 |\mathbf{00}\rangle\langle\mathbf{00}| + c_0(|\mathbf{01}\rangle\langle\mathbf{01}| + |\mathbf{10}\rangle\langle\mathbf{10}|) + d_0 |\mathbf{11}\rangle\langle\mathbf{11}| + e_0(|\mathbf{02}\rangle\langle\mathbf{02}| + |\mathbf{20}\rangle\langle\mathbf{20}|)$.

We now consider the entanglement swapping of two states of the form ρ_{success} . In the swap, an ensemble from each entangled pair is read out and the corresponding photons are combined on a balanced beam splitter. With probability a_0^2 , we are swapping two states of the form $|\Psi\rangle$ and the state after a successful swap is

$$\begin{aligned}
\rho_{a_0^2} = & \left[\frac{1}{4} \left[2\eta_{\text{dr}}(1 - \eta_{\text{dr}})(1 - P_{\text{dr}})^2 + 2(1 - \eta_{\text{dr}})^2P_{\text{dr}}(1 - P_{\text{dr}}) \right] |\mathbf{00}\rangle\langle\mathbf{00}| \right. \\
& + \frac{1}{4} \left[2P_{\text{dr}}(1 - P_{\text{dr}}) \right] |\mathbf{11}\rangle\langle\mathbf{11}| \\
& + \frac{1}{4} \left[2(1 - \eta_{\text{dr}})P_{\text{dr}}(1 - P_{\text{dr}}) \right] (|\mathbf{01}\rangle\langle\mathbf{01}| + |\mathbf{10}\rangle\langle\mathbf{10}|) \\
& + \frac{1}{2} \eta_{\text{dr}}(1 - P_{\text{dr}})^2 |\Psi\rangle\langle\Psi| \Big] \frac{1}{\mathcal{N}'}, \tag{S84}
\end{aligned}$$

where we have introduced the total readout detection efficiency η_{dr} , which is determined by the readout efficiency, the outcoupling losses and the efficiency of the detectors. In contrast to the detection efficiency in the entanglement generation, the readout detection efficiency does not include fiberlosses since the entanglement swap is a local process. \mathcal{N}' is a normalization constant. Furthermore, we have defined the readout dark count rate P_{dr} , which contains the probability of reading out incoherent photons from the ensembles and the detector dark counts, i.e. $P_{\text{dr}} = r_{\text{dark}}\tau_{\text{read}} + \eta_{\text{dr}}p_{\text{as}}$. Here $r_{\text{dark}}\tau_{\text{read}}$ is the dark count rate of the detectors and p_{as} is the probability to emit incoherent photons. As previously described p_{as} is mainly determined by the inefficiency of optical pumping in the initialization of the ensembles. From Eq. (S84), we can express $\rho_{a_0^2}$ as

$$\begin{aligned}
\rho_{a_0^2} = & \frac{1}{\mathcal{N}'} \left[\frac{1}{4} \alpha |\mathbf{00}\rangle\langle\mathbf{00}| + \frac{1}{4} (\beta - \eta_{\text{dr}}(1 - P_{\text{dr}})^2) (|\mathbf{01}\rangle\langle\mathbf{01}| + |\mathbf{10}\rangle\langle\mathbf{10}|) \right. \\
& + \frac{1}{4} \lambda |\mathbf{11}\rangle\langle\mathbf{11}| + \frac{1}{2} \eta_{\text{dr}}(1 - P_{\text{dr}})^2 |\Psi\rangle\langle\Psi| \Big], \tag{S85}
\end{aligned}$$

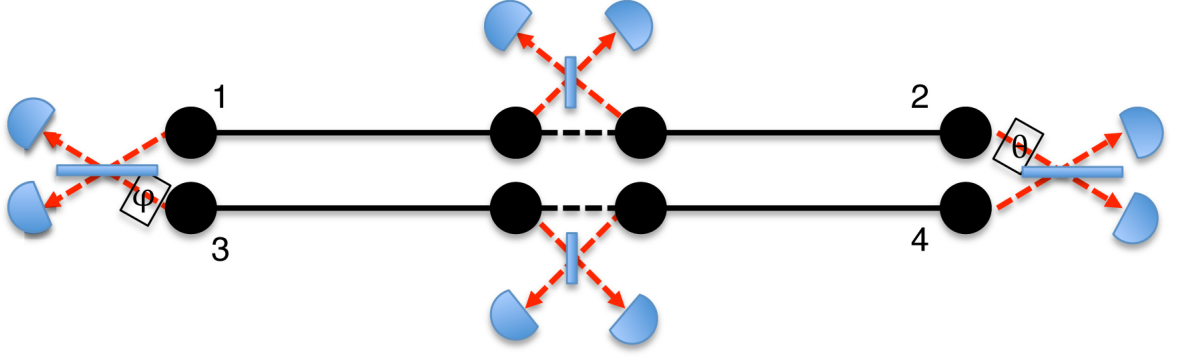


FIG. S9. Sketch of the postselection procedure after a single step of entanglement swapping (middle stations). The entanglement swaps creates entanglement between ensembles 1,2 and 3,4, respectively. Ensembles 1,2,3 and 4 are then read out and we condition on a single click at both stations. The phases ϕ and θ are ideally equal.

with α, β , and λ given by Eq. (S84). Considering all the combinations from swapping two states of the form ρ_{success} , we find that the output state can be written as

$$\begin{aligned} \rho_{\text{swap},1} = \frac{1}{\mathcal{N}''} & \left[\left[\frac{a_0^2}{4} \alpha + b_0^2 \lambda + c_0^2 \alpha + b_0 a_0 \beta + c_0 a_0 \alpha + 2b_0 c_0 \beta + 2b_0 e_0 \tilde{\beta} + 2c_0 e_0 \tilde{\alpha} + e_0^2 \tilde{\gamma} + a_0 e_0 \tilde{\alpha} \right] |\mathbf{00}\rangle \langle \mathbf{00}| \right. \\ & + \left[\frac{a_0^2}{4} (\beta - \eta_{\text{dr}}(1 - P_{\text{dr}})^2) + \frac{a_0 b_0}{2} \lambda + a_0 c_0 \beta + \frac{a_0 d_0}{2} \alpha + b_0 c_0 \lambda + b_0 d_0 \beta + c_0^2 \beta + c_0 d_0 \alpha \right. \\ & + \left. \left. \frac{a_0 e_0}{2} \tilde{\beta} + d_0 e_0 \tilde{\alpha} \right] (|\mathbf{01}\rangle \langle \mathbf{01}| + |\mathbf{10}\rangle \langle \mathbf{10}|) \right. \\ & + \left[\frac{a_0^2}{4} \lambda + c_0^2 \lambda + d_0^2 \alpha + c_0 a_0 \lambda + d_0 a_0 \beta + 2c_0 d_0 \beta \right] |\mathbf{11}\rangle \langle \mathbf{11}| \\ & + \left[\frac{a_0 e_0}{2} \beta + b_0 e_0 \lambda + c_0 e_0 \beta + 2e_0^2 \tilde{\beta} \right] (|\mathbf{02}\rangle \langle \mathbf{02}| + |\mathbf{20}\rangle \langle \mathbf{20}|) \\ & + \left[\frac{a_0 e_0}{2} \lambda + c_0 e_0 \lambda + d_0 e_0 \beta \right] (|\mathbf{12}\rangle \langle \mathbf{12}| + |\mathbf{21}\rangle \langle \mathbf{21}|) \\ & + e_0^2 \lambda |\mathbf{22}\rangle \langle \mathbf{22}| \\ & + \left. \frac{a_0^2}{2} \eta_{\text{dr}}(1 - P_{\text{dr}}) |\Psi\rangle \langle \Psi| \right], \end{aligned} \quad (\text{S86})$$

where we have defined

$$\tilde{\alpha} = 3\eta_{\text{dr}}(1 - \eta_{\text{dr}})^2(1 - P_{\text{dr}})^2 + 2(1 - \eta_{\text{dr}})^3 P_{\text{dr}}(1 - P_{\text{dr}}) \quad (\text{S87})$$

$$\tilde{\beta} = 2\eta_{\text{dr}}(1 - \eta_{\text{dr}})(1 - P_{\text{dr}})^2 + 2(1 - \eta_{\text{dr}})^2 P_{\text{dr}}(1 - P_{\text{dr}}) \quad (\text{S88})$$

$$\tilde{\gamma} = 4\eta_{\text{dr}}(1 - \eta_{\text{dr}})^3(1 - P_{\text{dr}})^2 + 2(1 - \eta_{\text{dr}})^4 P_{\text{dr}}(1 - P_{\text{dr}}), \quad (\text{S89})$$

and $\mathcal{N}'' = P_{\text{swap},1}$ is a normalization constant, which gives the success probability of the swap operation. It is seen that we can write

$$\begin{aligned} \rho_{\text{swap},1} = a_1 |\Psi\rangle \langle \Psi| + b_1 |\mathbf{00}\rangle \langle \mathbf{00}| + c_1 (|\mathbf{01}\rangle \langle \mathbf{01}| + |\mathbf{10}\rangle \langle \mathbf{10}|) + d_1 |\mathbf{11}\rangle \langle \mathbf{11}| + e_1 (|\mathbf{02}\rangle \langle \mathbf{02}| + |\mathbf{20}\rangle \langle \mathbf{20}|) \\ + f_1 (|\mathbf{12}\rangle \langle \mathbf{12}| + |\mathbf{21}\rangle \langle \mathbf{21}|) + g_1 |\mathbf{22}\rangle \langle \mathbf{22}| \end{aligned} \quad (\text{S90})$$

with constants $a_1, b_1, c_1, d_1, e_1, f_1$ and g_1 determined by Eq. (S86).

The vacuum part of the swapped state grows exponentially with the number of swaps in the DLCZ protocol [33] and it is therefore necessary to perform a final postselection where two entangled states are combined (see Fig. S9). We assume two parties named Alice and Bob who share two entangled pairs such that Alice has ensemble 1 and 3

and Bob has ensemble 2 and 4. Ensemble 1 and 2 are entangled and so is ensemble 3 and 4. The initial state is then

$$\begin{aligned} \rho_{\text{initial}} = & \left(a|\Psi\rangle\langle\Psi| + b|00\rangle\langle 00| + c(|01\rangle\langle 01| + |10\rangle\langle 10|) + d|11\rangle\langle 11| \right. \\ & \left. + e(|02\rangle\langle 02| + |20\rangle\langle 20|) + f(|12\rangle\langle 12| + |21\rangle\langle 21|) + g|22\rangle\langle 22| \right)_{1,2} \\ & \otimes \left(a|\Psi\rangle\langle\Psi| + b|00\rangle\langle 00| + c(|01\rangle\langle 01| + |10\rangle\langle 10|) + d|11\rangle\langle 11| \right. \\ & \left. + e(|02\rangle\langle 02| + |20\rangle\langle 20|) + f(|12\rangle\langle 12| + |21\rangle\langle 21|) + g|22\rangle\langle 22| \right)_{3,4} \end{aligned} \quad (\text{S91})$$

All ensembles are now readout in, e.g., a cryptography scheme and a success is conditioned on both Alice and Bob recording a single click. The total success probability is

$$\begin{aligned} P_{\text{ps}} = & \frac{a^2}{2}(\alpha_{\text{ps}}\beta_{\text{ps}} + \gamma_{\text{ps}}^2) + b^2\alpha_{\text{ps}}^2 + 2c^2\alpha_{\text{ps}}\beta_{\text{ps}} + d^2\beta_{\text{ps}}^2 + 2c^2\gamma_{\text{ps}}^2 + 2ab\alpha_{\text{ps}}\gamma_{\text{ps}} \\ & + 2ac(\alpha_{\text{ps}}\beta_{\text{ps}} + \gamma_{\text{ps}}^2) + 2ad\beta_{\text{ps}}\gamma_{\text{ps}} + 4bc\alpha_{\text{ps}}\gamma_{\text{ps}} + 4cd\beta_{\text{ps}}\gamma_{\text{ps}} + 2bd\gamma_{\text{ps}}^2 \\ & + 2ae(\alpha_{\text{ps}}\tilde{\beta}_{\text{ps}} + \gamma_{\text{ps}}\beta_{\text{ps}}) + 2af(\gamma_{\text{ps}}\tilde{\beta}_{\text{ps}} + \beta_{\text{ps}}^2) + 2ag\beta_{\text{ps}}\tilde{\beta}_{\text{ps}} + 4be\alpha_{\text{ps}}\beta_{\text{ps}} \\ & + 4bf\gamma_{\text{ps}}\beta_{\text{ps}} + 2bg\beta_{\text{ps}}^2 + 4ce(\gamma_{\text{ps}}\beta_{\text{ps}} + \alpha_{\text{ps}}\tilde{\beta}_{\text{ps}}) + 4cf(\beta_{\text{ps}}^2 + \gamma_{\text{ps}}\tilde{\beta}_{\text{ps}}) + 4cg\beta_{\text{ps}}\tilde{\beta}_{\text{ps}} + 4de\gamma_{\text{ps}}\tilde{\beta}_{\text{ps}} \\ & + 4df\beta_{\text{ps}}\tilde{\beta}_{\text{ps}} + 2dg\tilde{\beta}_{\text{ps}}^2 + 2e^2(\alpha_{\text{ps}}\tilde{\gamma}_{\text{ps}} + \beta_{\text{ps}}^2) + 4eg\beta_{\text{ps}}\tilde{\gamma}_{\text{ps}} + 4fg\tilde{\beta}_{\text{ps}}\tilde{\gamma}_{\text{ps}} + g^2\tilde{\gamma}_{\text{ps}}^2 \\ & + 4fe(\gamma_{\text{ps}}\tilde{\gamma}_{\text{ps}} + \tilde{\beta}_{\text{ps}}\beta_{\text{ps}}) + 2f^2(\tilde{\gamma}_{\text{ps}}\beta_{\text{ps}} + \tilde{\beta}_{\text{ps}}^2), \end{aligned} \quad (\text{S92})$$

where we have defined

$$\alpha_{\text{ps}} = 2P_{\text{dr}}(1 - P_{\text{dr}}) \quad (\text{S93})$$

$$\beta_{\text{ps}} = 2\eta_{\text{dr}}(1 - \eta_{\text{dr}})(1 - P_{\text{dr}})^2 + 2(1 - \eta_{\text{dr}})^2P_{\text{dr}}(1 - P_{\text{dr}}) \quad (\text{S94})$$

$$\gamma_{\text{ps}} = \eta_{\text{dr}}(1 - P_{\text{dr}})^2 + 2(1 - \eta_{\text{dr}})P_{\text{dr}}(1 - P_{\text{dr}}) \quad (\text{S95})$$

$$\tilde{\beta}_{\text{ps}} = 3\eta_{\text{dr}}(1 - \eta_{\text{dr}})^2(1 - P_{\text{dr}})^2 + 2(1 - \eta_{\text{dr}})^3P_{\text{dr}}(1 - P_{\text{dr}}) \quad (\text{S96})$$

$$\tilde{\gamma}_{\text{ps}} = 4\eta_{\text{dr}}(1 - \eta_{\text{dr}})^3(1 - P_{\text{dr}})^2 + 2(1 - \eta_{\text{dr}})^4P_{\text{dr}}(1 - P_{\text{dr}}). \quad (\text{S97})$$

The postselected fidelity of the state is

$$F_{\text{ps}} = \frac{\frac{a^2}{4}\eta_{\text{read}}^2\eta_{\text{dr}}^2(1 - P_{\text{dr}})^4(1 + \cos(\phi - \theta)) + \frac{a^2}{4}(\gamma_{\text{ps}}^2 - \eta_{\text{read}}^2\eta_{\text{dr}}^2(1 - P_{\text{dr}})^4) + c^2\gamma_{\text{ps}}^2 + ac\gamma_{\text{ps}}^2}{P_{\text{ps}}}, \quad (\text{S98})$$

where the phases ϕ, θ can be different due to variations in the path lengths of the photons being read out. In the ideal case, we have $\phi = \theta$ for which the fidelity is maximal. The rate of a DLCZ repeater based on the room temperature cells can be estimated as [33]

$$r \approx \left(\frac{2}{3}\right)^{n+1} P_0 P_{\text{swap},1} P_{\text{swap},2} \dots P_{\text{swap},n} P_{\text{ps}} \frac{2^n c}{L} \quad (\text{S99})$$

where n is the number of swap levels in the repeater and L is the distance. Note, however, that the scalability of the room temperature cells enables spatially multiplexing, which both increases the rate of the repeater and decreases the necessary memory time of the ensembles [33]. Assuming that $2M$ ensembles are used at each repeater station, the rate will increase by a factor of M . We have considered a basic repeater segment consisting of only a single swap without multiplexing in order to estimate the rate and fidelity of a distributed pair. We assume that the distance to distribute entanglement over is $L = 80$ km and that the losses in the fibers are given by the attenuation length at telecom wavelengths, which is ~ 20 km. Furthermore, we assume SPD efficiencies of 95% and dark count rates of 1 Hz. This reflects what is possible with current superconducting detectors [22, 23]. We then perform an optimization in all the parameters characterizing the cells, e.g. the excitation probability, the write time and the readout time. We include experimental imperfections such as outcoupling losses of around 10% and intracavity losses of 2%. As a result we find that a pair with fidelity $\sim 80\%$ can be distributed with a rate of ~ 0.2 Hz. We have assumed that $p_{\text{pump}} \approx 0.08\%$ and have neglected effects from finite memory time of the atoms. Furthermore, we have assumed that $\phi = \theta$ (see Fig. S9). This rate can, however, be greatly enhanced using spatial multiplexing which is possible with this kind of system. This will also decrease the necessary coherence time of the atoms [15].